UNIVERSITY OF CALIFORNIA SAN DIEGO

Light-driven Nanomotors/robots for Environmental and Biomedical Applications

A dissertation submitted in partial satisfaction of the

requirements for the degree Doctor of Philosophy

in

Materials Science and Engineering

by

Weichen Wei

Committee in charge:

Professor Joseph Wang, Chair
Professor Shengqiang Cai
Professor Irene Litvan
Professor Sheng Xu
Professor Liangfang Zhang

2022

The dissertation of Weichen Wei is approved, and it is acceptable in quality and form for publication on microfilm and electronically.

University of California San Diego

2022

DEDICATION

This dissertation is dedicated to my Ph.D. advisor and my scientific hero, Prof. Joseph Wang, who has been very loving, kind, and thoughtful to help me improve constantly throughout my Ph.D. journey.

This dissertation is also dedicated to my parents, who raised me with tremendous meticulousness in every possible way. I am truly blessed and forever grateful to have them in my life. All my work would never happen without their support and efforts.

I am hugely grateful forever for all my mentors and friends, who have given me everlasting and overwhelming help to accompany and support me in front of extreme hardship.

EPIGRAPH

Keep smiling

Spread kindness

Make good reactions happen

Never give up

Strengthen self without stopping, and hold world with virtue.

Dream as I will live forever, and live as I will die today.

TABLE OF CONTENTS

LIST OF FIGURES

ACKNOWLEDGEMENTS

First and foremost, I would like to thank my Ph.D. advisor, Professor. Joseph Wang for his kind guidance and support throughout my Ph.D. journey. I am super grateful for the opportunity he provided for me to work with my scientific hero, and to learn and grow with the brothers and sisters from various countries in the NBE team. With his profound understanding of science and insightful teaching for me, I had a chance to be familiar with how to convert knowledge to really useful applications.

I would also like to thank all my committee members, to whom I owe much of my success. Over the years, They provided a huge amount of support for my academic life here.

I would also like to thank my lovely and helpful labmates. Together we make great progress and give a hand to each other. Last but not least, I would like to thank UC San Diego. In particular, the JSOE and Mat Sci faculty and staff have consistently supported me in the academic life.

VITA

2018 B.S. in Chemistry, University of Science and Technology of China, China

2022 Ph.D. in Materials Science and Engineering, University of California San Diego, USA

ABSTRACT OF THE DISSERTATION

Light-driven Nanomotors/robots for Environmental and Biomedical Applications

by

Weichen Wei

Doctor of Philosophy in Materials Science and Engineering

University of California San Diego, 2022

Professor Joseph Wang, Chair

In recent years, micro/nanomotors have become an important research field in nanotechnology. Light-driven micro/nanomotors have received extensive attention due to the advantages of high controllability, good programmability, and easy operation, as well as their potential in environmental remediation and biomedical applications.

Herein, Chapter 1 introduces the background and motion mechanism of the field of light-driven micro/nanomotors, the design principles of light-driven micro/nanomotor materials, and the motion modes of individual motors and group motors. In addition, the current development and applications in this field are also discussed. The second chapter of the dissertation will focus on the work of applying single-atom catalysis to enhance the performance of nanomotors and the related application. The third chapter of the dissertation will discuss the work of developing light-driven $SrTiO_3$:Al-based nanomotors for antimicrobial applications. The last chapter of the dissertation will summarize the conclusion of this dissertation and serve as a paradigm to rationally design novel light-driven nano/micromotors based on cutting-edge photocatalysts with outstanding catalytic performance for potential environmental and biomedical applications

Chapter 1

Introduction

1.1 Background of Light-driven Nano/micromotors

Light-driven nano/micromotors exhibit some unique advantages. As an external field, light can precisely tune and input energy by adjusting parameters such as light intensity, light frequency, polarization degree, and propagation direction. Therefore, light-driven nano/micromotors have the advantages of high controllability, good programmability, and easy operation. In addition, the development of photocatalysis has also injected vitality into the field of light-driven nano/micromotors [1-4].

A light-driven micro/nanomotor is a micro/nanoscale actuator that converts light energy into mechanical energy. According to Newton's third law, the fabrication of light-driven micro/nanomotors requires: (1) photo-responsive materials; (2) a local asymmetric gradient field around the motor under illumination; (3) a hydrodynamic direct action under illumination for micro/nanomotors. Under light stimulation, the light-driven micro/nanomotor system exhibits non-equilibrium photoresponse in all surrounding directions. Based on the response behavior (photochemical reaction, temperature change, interfacial tension change, deformation, etc.), the formed non-equilibrium gradient field or non-equilibrium force will drive the nano/micromotor in the fluid environment [5].

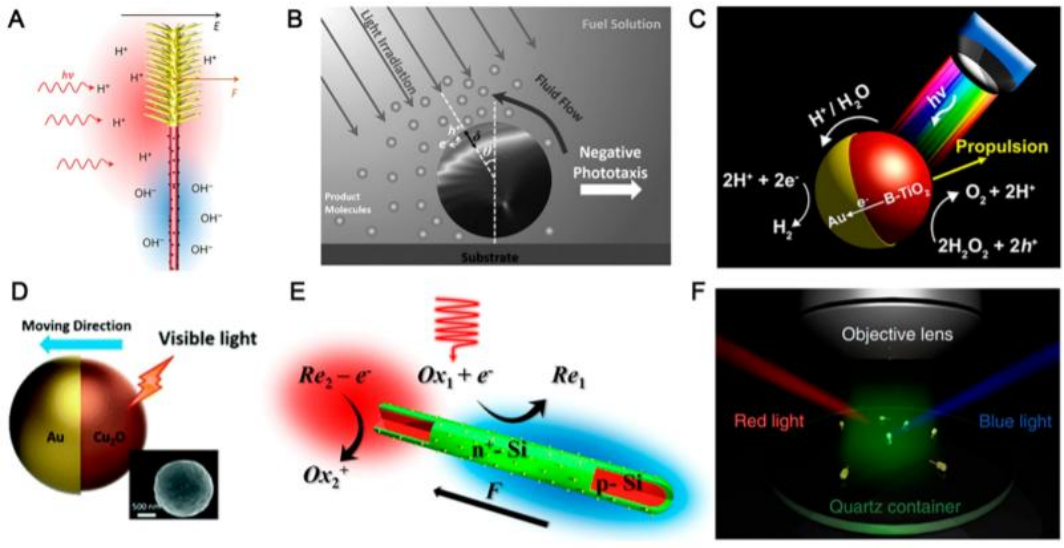

Figure 1.1 Demonstrations of typical controllable light-driven micro/nanomotors ref.1 Copyright 2018, American Chemical Society

The successful fabrication of light-driven micro/nanomotors relies on light-responsive materials. Depending on the properties of the light-responsive materials, different photoresponsive behaviors occur under illumination, roughly classified into photochromic, photothermal, photolysis, and photocatalytic materials.

Photochromic materials are a class of light-responsive materials that change their molecular structure and reversibly change their color when exposed to light. After removing the light source or irradiating the photochromic materials with the light of different wavelengths, they can switch back to the original molecular structure. Spiropyrans, azobenzenes and their derivatives have good chemical stability, and high photochemical reaction efficiency. They can undergo cis-trans isomerization, pericyclization and other reactions under light, thereby generating surface free energy or hydrophilicity change on light-responsive surfaces [6-14]. Motors driven by interfacial tension gradients are most commonly used to fabricate light-driven micro/nanomotors.

Photothermal materials can effectively absorb light energy and convert it into heat energy, rapidly increase the temperature of the surrounding environment of the photothermal materials, and generate an asymmetric temperature gradient field to drive the motor to move forward. The photothermal conversion efficiency depends on the metal composition, the size and shape of nanoparticles, the dielectric properties of the surrounding medium, and the interaction between particles. Compared with ultraviolet light, near-infrared light can penetrate the skin and has good biosafety, and the micro/nanomotors prepared from such materials show great potential in the fields of drug delivery and photothermal therapy [15-24].

Photodecomposable materials, such as some inorganic salts (AgCl solution), will be decomposed under light to produce H^+ and Cl^- with different ionic diffusion coefficients. In a fluid environment, the diffusion rate of H^+ is much higher than that of Cl^-, which will be in the micromotor. An electrolyte

concentration gradient field is formed in the surrounding medium, and the micro/nanomotor is driven by the mechanism of electrophoresis and electroosmosis [25-28].

Photocatalytic materials are mainly composed of metal and oxide semiconductors (such as TiO_2, BiOI, CuO, ZnO), and are currently the most common materials used to fabricate light-driven micro/nanomotors [29-31]. The photocatalytic efficiency can be effectively improved by accelerating the charge transfer and confining the recombination process of electron-hole pairs, such as the use of hole scavengers or composite photocatalysts coupled with metals, which favor the formation of bubbles and/or concentration gradients, thereby enhancing the photocatalytic efficiency.

1.2 Mechanism of Light-driven Nano/micromotors

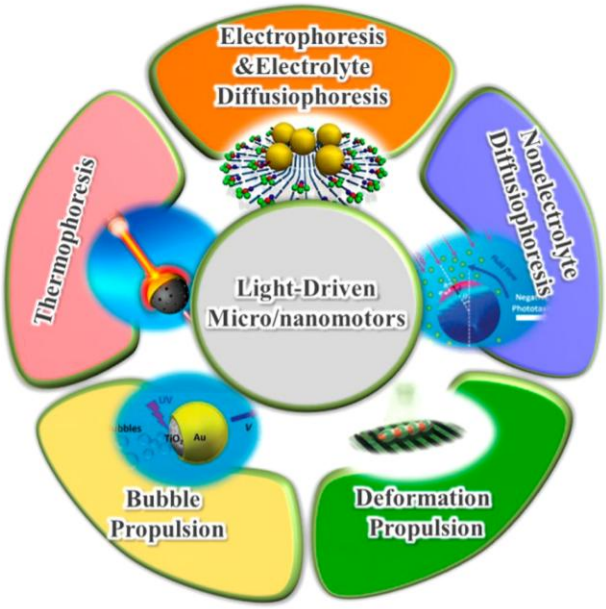

Figure 1.2 Light-driven micro/nanomotors propelled by different mechanisms ref.1 Copyright 2018, American Chemical Society

Common light-driven micro/nanomotor geometries are wire, rod, Janus sphere, tube, and gear. Asymmetric shape or surface anisotropic light-responsive micro/nanomotors will lead to uneven distribution of photochemical reaction products or light-induced surrounding energy fields, which is conducive to the establishment of gradient fields with asymmetric concentration, temperature and other physical quantities.

In addition to constructing asymmetric geometries, an asymmetric field around a micro/nanomotor can also be created by manipulating an external light field. Asymmetric light stimulation exerts a non-uniform light field around the motor, which can drive either shape-symmetric or isotropic light-driven micro/nanomotors. For another example, nanomotors coated with azobenzene can achieve high-speed directional motion in aqueous solutions under light intensity gradients. Photochromic molecules undergo excitation and relaxation cycles of trans-cis-trans isomers under illumination, and an increase in illumination intensity leads to an increase in the number of cycles of photoisomerization, which forms interfacial tension gradient providing enough power for the motor to accelerate toward the dark area. In addition, structural light illumination can also create a non-uniform light field around the micro/nanomotors. Through the optical projection system of the digital micromirror device, the light field distribution and light intensity projected to the working area of the micro/nanomotors can be regulated in space and time. The micro/nanomotors is fabricated from the photodeformable material LCE, only the part exposed to light will deform, so structured light can induce asymmetric deformation of the micro/nanomotors, thereby promoting the directional motion of the micro/nanomotors [32-33].

The fluid propulsion forces directly acting on light-driven micro/nanomotors include bubble propulsion and light-responsive elastic deformation propulsion. Light-driven micro/nanomotors driven by the propulsion of bubbles generally adopt Janus spheres or tubular structures, and generate gas molecules through photochemical reactions under light. The bubbles nucleate, grow, and eject to provide the driving force for the motor to push it forward. On the other hand, the light-driven micro/nanomotors prepared from light-responsive deformable LCE materials undergo reversible photoisomerization reaction under specific wavelengths of illumination, transition between anisotropy and isotropy, and the liquid crystal system undergoes a phase transition. The deformation is generated, and macroscopically, it shrinks along the direction of the pointing vector and outputs the driving force. The motion range of the micro/nanomotor belongs to the low Reynolds number system, so the viscous force and the Brownian motion of the particles have a great influence on it. In order to overcome the

viscous resistance in the fluid, light-driven micro/nanomotors need a continuous driving force to maintain their motion. The motor motion triggered by light stimulation originates from the asymmetric structure or the asymmetric concentration gradient field or the non-equilibrium hydrodynamic force established under non-uniform illumination conditions, breaking the symmetry of the pressure distribution is the principle of driving the motor. According to the nature of the light-driven force, the motion mechanisms of light-driven micro/nanomotors are divided into light-induced bubble propulsion, self-electrophoresis, self diffusiophoresis, autothermophoresis, interfacial tension gradient propulsion, and deformation propulsion [34].

In a typical photocatalytic oxygen production system, when a micro/nanomotor prepared from photocatalytic materials (such as TiO_2 and WO_3) is stimulated by light, a photocatalytic reaction will occur on its surface to decompose H_2O_2 to generate high concentrations of oxygen. Bubble propulsion is realized by the microjets generated when the bubbles grow and collapse on the surface of the micro/nanomotor and the impulse generated by the bubbles detaching from the surface of the motor. The efficient accumulation of gas to nucleate to form microbubbles before oxygen diffuses to the surroundings is the key to the bubble propulsion mechanism, and photocatalytic materials with high apparent quantum efficiency or relatively space-constrained tubular micro/nanomotors can be effective inhibit the diffusion of oxygen molecules. By remotely adjusting the on/off mode of the light source and changing the light irradiation intensity, the start-stop control and speed control of the bubble-propulsion light-driven micro/nanomotor motion (light response time < 0.1 s) can be realized.

Self-electrophoresis refers to the movement of a charged micro/nanomotor in a self-generated electric field. Asymmetric disproportionation reaction occurs on the surface of a micro/nanomotor prepared from photocatalytic materials under light stimulation, and a redox reaction occurs on one side to generate ions, and the other side generates ions. The ions are consumed on one side, and an asymmetric ion concentration distribution is formed around the motor. The established electrolyte gradient forms a local self-generated electric field, which drives the overall charged micro/nanomotor to

move. The direction of movement depends on the type of surface charge and the Zeta potential of the motor [35-37].

An asymmetric concentration gradient field is formed around the micro/nanomotor induced by light, which causes the spontaneous motion of dispersed particles in the fluid, which is called self diffusiophoresis [38-39]. The products used to construct the concentration gradient field can be divided into two types: electrolyte and non-electrolyte type. The form of the electric field in electrolyte self diffusiophoresis is different from that in self-electrophoresis. For self-electrophoresis, photochemical reactions occur between the anode and cathode that are spatially separated from each other under light, and the formed ionic products are enriched in different areas of the motor surface, thereby The gradient electric field is formed inside the motor, which is essentially an internal gradient field. For electrolyte self diffusiophoresis, the anodic and cathodic reactions take place in a local space, and the generated ions are locally distributed on one side of the motor and dissociate from the surrounding fluid in the form of ions. The migration velocity diffuses outward to form a concentration gradient, thereby generating a diffusion-induced electric field, which is essentially an external gradient field. Similar to the photogenerated electrolyte concentration gradient, photocatalytic reactions can also occur on the surface of the micro/nanomotor to generate neutral molecules to construct a non-electrolyte concentration gradient. By using asymmetric photocatalytic structures or providing asymmetric illumination conditions on isotropic photocatalysts, an asymmetric photocatalytic reaction occurs to construct a non-electrolyte concentration gradient. In neutral molecule-mediated diffusion electrophoresis, the asymmetric pressure gradient formed by the interaction between the molecules generated by the photochemical reaction and the motor surface acts as an osmotic force to drive the motion of the micro/nanomotor.

Light-induced asymmetric temperature gradients can drive micro/nanomotors through the mechanism of thermophoresis, and utilize the properties of photothermal materials to absorb and convert light energy into thermal energy to build a temperature gradient around the micro/nanomotors

[40-42]. Photothermal particles with symmetric geometries usually exhibit Brownian motion under illumination due to the mutual cancellation of thermophoretic forces due to symmetric thermal diffusion. Therefore, most micro/nanomotors driven by light-induced temperature gradients adopt asymmetric geometries and cover part of the sphere with photothermal materials. The part of the material with thermal effect heats up rapidly under light conditions, while the part of the material without thermal effect heats up slowly, resulting in a continuous temperature gradient under continuous light stimulation. The fluid temperature needs to reach equilibrium. The water flow in the low temperature part of the motor will flow around the surface of the motor to the high temperature part, and the reaction force of the water flow drives the motor.

The interfacial tension is an elastic force trend of the fluid interface. Since the high tension fluid has a greater force on the surrounding medium than the low tension fluid, the interfacial tension gradient will cause the fluid to flow from the low tension area to the high tension area, so it is induced under illumination. The interfacial tension gradient of the micro/nanomotor can make it move. The interfacial tension is determined by the properties of the outermost surface that is in direct contact with the fluid. Under light stimulation, the outermost molecules can undergo different photochemical reactions due to different chemical structures, changing the Interface characteristics in contact with fluids. Photochromic materials such as azobenzene and its derivatives, their cis-trans isomers exhibit reversible changes in physicochemical properties under illumination, such as dipole moment and affinity for polar molecules. Using this feature, we can control interfacial properties, including surface tension and wettability, to design light-driven nanomaterials based on local interfacial tension gradients [43].

In the absence of external stimuli, LCE shows the orientation of nematic liquid crystals and has reversible expansion; Under external stimuli such as heat and light, the liquid crystal behaves isotropically, shrinking along the arrangement direction of the mesogen, causing the shape change. This reversible expansion and contraction generates torque to make the LCE fluid, inducing movement of the LCE upon light stimulation [44].

1.3 Motion behavior of Light-driven Nano/micromotors

For all types of light-driven micro/nanomotors, their motion patterns and motion regulation are the keys to study. Recent progress has shown that some novel light-driven micro/nanomotors can achieve directional motion by remote control. Depending on the preparation components of light-driven micro/nanomotors, light of a specific wavelength is usually required to activate and control the motion of the motor. Near-infrared light, visible light, and ultraviolet light are often used as light sources to drive micro/nanomotors. Under illumination, light-driven micro/nanomotors can exhibit different motion patterns. The motion speed and motion direction are two important parameters for evaluating the motion characteristics of the motor. The start and stop of the motion can be quickly regulated by the on/off mode of the light source, and the motion speed is affected by the incident light intensity, the type and concentration of the substance in the solution. Light-driven micro/nanomotors can exhibit the directional motion and rotation of individual motors, and the motion trajectories of the motors can be remotely controlled by moving the position of the light source. It can also imitate the movement behavior of organisms in nature, manifesting as the directional movement, aggregation and disaggregation of swarm motors.

The motion start-stop control of light-driven micro/nanomotors can be remotely controlled by the on/off mode of the light source, which has the characteristics of strong operability, good repeatability and fast response speed. The motion speed of the light-driven micro/nanomotor is also positively correlated with the intensity of the incident light source and the concentration of the solution. By adjusting the intensity of the light source and the concentration of chemical fuel in the solution, the motor speed can be precisely regulated. In addition, the motion of light-driven micro/nanomotors exhibits stability, repeatability, and persistence. Even after multiple cycles of on/off control, the motor exhibits a small change in the maximum speed of motion that is not damaged by repeated illumination.

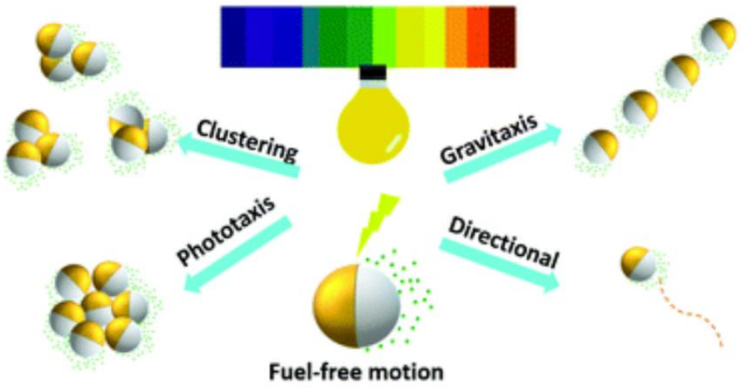

Figure 1.3 Light-driven micro/nanomotors with different motion behaviors ref.30 Copyright 2019, Royal Society of Chemistry

The motion characteristics of light-driven micro/nanomotors can be divided into two categories: individual and group motion patterns [45-46]. According to different preparation shapes, parameters, physical or chemical modification components, and relative positions of light sources, individual motors can realize remote control of the movement direction and movement trajectory. Swarm motors exhibit aggregation and disaggregation phenomena under illumination, and perform directional movements in the form of swarms. Using this feature, the desired particle population and geometry can be obtained by changing parameters such as light intensity or particle size, and a multifunctional micro/nanomotor cluster system can be designed to perform more complex cooperative tasks. The motion of individual motors mainly has two forms: directional motion and rotation. After the construction of an asymmetric gradient field or the application of direct hydrodynamic forces, most micro/nanomotors with geometric configurations perform directional motion. Using the positive/negative phototaxis of light-driven micro/nanomotors, the motion direction of the motor can be controlled more precisely. Rotational motion is the motion characteristic of gear-like light-driven micro/nanomotors, which can effectively convert the light energy absorbed by the gears into mechanical energy of rotational motion under light stimulation.

The swarm motor mainly includes aggregation, disaggregation motion, and directional motion after swarming. The aggregation phenomenon is caused by the diffusional migration mediated by the

photochemical concentration gradient. After the individual motors gather to form a group, the positive/negative phototaxis of the group motor can be used to control its directional movement under light [47-48].

1.4 Light-driven Nano/micromotors for Environmental and Biomedical Applications

1.4.1 Light-driven Nano/micromotors for Environmental Applications

On the basis of a large number of studies on the characteristics of light-diven nano/micromotors, the research on the environmental remediation of light-controlled nano/micromotors is increasing [22-23]. The researchers used the uniqueness of photocatalytic materials to prepare high-efficiency, stable and controllable light-controlled nano/micromotors to achieve desirable removal of pollutants in water without external stirring.

TiO_2-based light-driven nano/micromotors have the advantages of the most widely used, cheap, stable, non-toxic and harmless, and have good photocatalytic oxidation performance to pollutants under illumination [49]. However, due to its wide band gap, most TiO_2 nano/micromotors mostly only show good response under UV light. And most of these motors currently have the defects of complicated preparation process and expensive preparation cost, which are not conducive to mass production and practical application.

In addition to TiO_2, C_3N_4, ZnO, Bi_2O_3, WO_3, etc. have all been used as common photocatalytic materials in the preparation of light-driven nano/micromotors. These materials have unique application advantages, such as good response to visible light, easy preparation, and magnetic properties. Therefore, using it for the preparation of light-driven nano/micromotors can improve the utilization efficiency of light energy and the yield of nano/micromotors, thereby increasing the possibility of the application of light-driven nano/micromotors in environmental remediation.

The light-driven nano/micromotors can effectively use light energy for driving and motion control without additional stirring. By realizing the autonomous movement of light-driven nano/micromotors, the material contact efficiency is improved, thereby effectively improving the degradation efficiency of pollutants in the water body, and it has a great application prospect in the field of environment, especially in the field of water body remediation. However, there are still some problems and limitations, so there is a large research space and significance. Light-driven nano/micromotors have high requirements on reaction conditions. At present, most of the research on the motion of nano/micromotors is limited to H_2O_2 solution, deionized water or single pollutant system, and only a small part of the research on its motion in seawater, lake water, milk and other foods. In addition, light-driven nano/micromotors also have problems such as too narrow utilization of light waves and poor biocompatibility. In order to ensure the environmental remediation ability of the light-driven nano/micromotors under visible light illumination at room temperature, and break the limitations of UV light in practical applications, the nano/micromotors can be prepared by combining with novel photocatalytic materials, or the nano/micromotors can be reasonably modified. Therefore, it is of great significance to test the water remediation ability of light-driven nano/micromotors in actual water bodies and multi-wavelength illumination conditions, while reducing the use of chemical fuels and preparing truly green and efficient water remediation materials. Furthermore, the fabrication process of light-driven nano/micromotors is complicated. At present, most of the light-driven nano/micromotors often use precious metal deposition, surface modification and other methods to achieve directional movement, removal of specific pollutants and other functions. However, there are problems that the preparation method is too complicated, and the raw film materials are expensive (such as Au, Pt) [50], which leads to high cost and is not suitable for mass production. This greatly hinders its application and promotion in the field of environmental remediation. In addition, light-driven nano/micromotors based on two-dimensional materials such as graphene, Mxene, transition metal dichalcogenides, etc. have shown great potential in the environmental remediation due to their unique structural and chemical properties [51-52]. It is the future development goal of this field to prepare green, cheap, autonomous

and precise photocontrolled micro and nano motors with good biocompatibility and pollutant removal ability in pure water system in the simplest and suitable for mass production.

1.4.2 Light-driven Nano/micromotors for Biomedical Applications

The advantages of light-driven micro/nanomotors, such as remote controllability, adjustable speed, and fast response, endow them with the ability to move according to specified trajectories, find targets by themselves, and local heating, etc., making them show excellent application prospects in the field of biomedicine, including Substance transport and separation, photothermal therapy, transmission of biochemical signals [1].

Light-driven micro/nanomotors, capable of loading and transporting goods, are one of the most important applications of micro/nanomotors and have broad application prospects in the field of micro/nanoengineering. Micro/nanomotors with hollow mesoporous structures have good ability of drug binding and loading, the active diffusion of nanomotors is excited under the irradiation of near-infrared light, the remote control of the motor to move away from the light source toward the target position, and the control of the distance of drug transport from left to right by changing the power of near-infrared light [53-55].

It can be seen that by turning on/off the light source to approach, capture, transport, and release particles to the final target area, the light-driven micro/nanomotor has the ability to load and transport substances/drugs. It is activated under illumination and follows a predetermined path. By adjusting the intensity and direction of the incident light, the movement speed and trajectory of the microspheres can be easily, quickly and precisely controlled, and efficient material transport can be achieved under real-time optical navigation.

Photothermal therapy is a treatment method that uses materials with high photothermal conversion efficiency, which are injected into the body, gathered near tumor tissues with targeted recognition technology, and converted into heat energy under the irradiation of external light sources to kill cancer

cells. Near-infrared light penetrates biological tissues most effectively, and does not produce the same effects on biological tissues as ultraviolet light. Therefore, it has great application potential in the field of disease treatment of light-driven micro/nanomotors. It is worth mentioning that although photothermal motors in the first near-infrared region have been reported, there are few studies on photothermal motors in the second near-infrared region. It is an important goal to broaden the range of usable spectrum, optimize the photoresponse ability of light-driven micro/nanomotors to multiple wavelength ranges, and improve the light absorption and light conversion ability to achieve the expected light driving efficiency [18, 56-57].

Berns designed a light-driven rotating micromotor to exert a shear force on the growth cone of a neuron by controlling the local microflow generated by its rotation. The growth cone rotates in response to the direction of the shear force [58]. Since the behavior of the growth cone pair at the top of the axon determines the direction of axon growth and migration, the direction of neuronal axon growth can be precisely regulated by changing the rotation direction of the light-driven micromotor and its relative position with the neuron, and the neuronal axon reprogramming can be induced. The rotation of the micromotor is realized by the adjustment of the light field, and the micromotor rotates clockwise or counterclockwise at a specific rate through the angular momentum of polarized light. It can make a "left" or "right" response, and by changing the rotation direction and position of the micromotor, a quick switch between different directional effects can be achieved. Light-driven micro/nanomotors realize the transmission of biochemical signals by exerting lateral force on biological cells, which provides a basis for the realization of light-induced directional remodeling of a large number of axons, which may be used in vivo to guide regeneration axes synaptogenesis-mediated repair of the brain and spinal cord. This phenomenon has potential applications not only in neurons, but also in other cell migration systems with similar signal transduction pathways. In addition, light-driven micromotors with the ability to adsorb toxins can be used for the removal of harmful substances such as toxins, biological metabolites,

and heavy metals in the intracellular and extracellular environments of organisms for active and multifunctional detoxification.

At present, most light-driven micro/nanomotors achieve propulsion in H_2O_2 and H_2O solutions, however, the biological toxicity of H_2O_2 severely limits the application scope of light-driven micro/nanomotors. Although H_2O is an ideal driving environment, the motor speed in pure water still needs to be improved, especially in viscous liquids, electrolyte solutions, flowing liquids (such as hydrogels or blood), where the driving power is low and the operating environment is relatively restricted. In addition, although NIR-driven micro/nanomotors with high biosafety show good bioclinical application potential, such motors often require strong NIR to be driven. The long-term, high-intensity light that the light-driven motors are exposed to during the task will cause severe thermal effects, and it will lead to potential biosafety issue and this requires further systematic research.

1.5 References

(1) Wang, J.; Xiong, Z.; Zheng, J.; Zhan, X.; Tang, J. Light-Driven Micro/Nanomotor for Promising Biomedical Tools: Principle, Challenge, and Prospect. *Acc. Chem. Res*. **2018**, 51 (9), 1957-1965.

(2) Xu, L.; Mou, F.; Gong, H.; Luo, M.; Guan, J. Light-Driven Micro/Nanomotors: From Fundamentals to Applications. *Chem. Soc. Rev*. **2017**, 46 (22), 6905-6926.

(3) Dong, R.; Cai, Y.; Yang, Y.; Gao, W.; Ren, B. Photocatalytic Micro/Nanomotors: From Construction to Applications. *Acc. Chem. Res*. **2018**, 51 (9), 1940-1947.

(4) Šípová-Jungová, H.; Andrén, D.; Jones, S.; Käll, M. Nanoscale Inorganic Motors Driven by Light: Principles, Realizations, and Opportunities. *Chem. Rev*. **2020**, 120 (1), 269-287.

(5) Dai, B.; Zhou, Y.; Xiao, X.; Chen, Y.; Guo, J.; Gao, C.; Xie, Y.; Chen, J. Fluid Field Modulation in Mass Transfer for Efficient Photocatalysis. *Adv. Sci*. **2022**, 9 (28), e2203057.

(6) Moo, J. G. S.; Presolski, S.; Pumera, M. Photochromic Spatiotemporal Control of Bubble-Propelled Micromotors by a Spiropyran Molecular Switch. *ACS Nano* **2016**, 10 (3), 3543-3552.

(7) Zhang, Q.; Dong, R.; Chang, X.; Ren, B.; Tong, Z. Spiropyran-Decorated SiO_2-Pt Janus Micromotor: Preparation and Light-Induced Dynamic Self-Assembly and Disassembly. *ACS Appl. Mater. Interfaces* **2015**, 7 (44), 24585-24591.

(8) Ye, Z.; Wang, Y.; Liu, S.; Xu, D.; Wang, W.; Ma, X. Construction of Nanomotors with Replaceable Engines by Supramolecular Machine-Based Host-Guest Assembly and Disassembly. *J. Am. Chem. Soc*. **2021**, 143 (37), 15063-15072.

(9) Tu, Y.; Peng, F.; Heuvelmans, J. M.; Liu, S.; Nolte, R. J. M.; Wilson, D. A. Motion Control of Polymeric Nanomotors Based on Host-Guest Interactions. *Angew. Chem. Int. Ed*. **2019**, 58 (26), 8687-8691.

(10) Li, W.; Wu, X.; Qin, H.; Zhao, Z.; Liu, H. Light-Driven and Light-Guided Microswimmers. *Adv. Funct. Mater*. **2016**, 26 (18), 3164-3171.

(11) Lin, X.; Xu, B.; Zhao, Z.; Yang, X.; Xing, Y.; You, C.; Kong, Y.; Cui, J.; Zhu, L.; Lin, S.; Mei, Y. Flying Squirrel-Inspired Motion Control of a Light-Deformed Pt-PAzoMA Micromotor through Drag Force Manipulation. *ACS Appl. Mater. Interfaces* **2021**, 13 (25), 30106-30117.

(12) Mena-Giraldo, P.; Orozco, J. Photosensitive Polymeric Janus Micromotor for Enzymatic Activity Protection and Enhanced Substrate Degradation. *ACS Appl. Mater. Interfaces* **2022**, 14 (4), 5897-5907.

(13) Abid, J.-P.; Frigoli, M.; Pansu, R.; Szeftel, J.; Zyss, J.; Larpent, C.; Brasselet, S. Light-Driven Directed Motion of Azobenzene-Coated Polymer Nanoparticles in an Aqueous Medium. *Langmuir* **2011**, 27 (13), 7967-7971.

(14) Xiong, X.; Huang, X.; Liu, Y.; Feng, A.; Wang, Z.; Cheng, X.; He, Z.; Wang, S.; Guo, J.; Yan, X. Azobenzene-Bearing Polymer Engine Powered Organic Nanomotors for Light-Driven Cargo Transport. *Chem. Eng. J*. **2022**, 445, 136576.

(15) Xuan, M.; Wu, Z.; Shao, J.; Dai, L.; Si, T.; He, Q. Near Infrared Light-Powered Janus Mesoporous Silica Nanoparticle Motors. *J. Am. Chem. Soc*. **2016**, 138 (20), 6492-6497.

(16) Cao, S.; Shao, J.; Wu, H.; Song, S.; De Martino, M. T.; Pijpers, I. A. B.; Friedrich, H.; Abdelmohsen, L. K. E. A.; Williams, D. S.; van Hest, J. C. M. Photoactivated Nanomotors via Aggregation Induced Emission for Enhanced Phototherapy. *Nat. Commun*. **2021**, 12 (1), 2077.

(17) Choi, H.; Lee, G.-H.; Kim, K. S.; Hahn, S. K. Light-Guided Nanomotor Systems for Autonomous Photothermal Cancer Therapy. *ACS Appl. Mater. Interfaces* **2018**, 10 (3), 2338-2346.

(18) Fu, S.; Fu, D.; Xie, D.; Liu, L.; Chen, B.; Ye, Y.; Wilson, D. A.; Peng, F. Light Driven Micromotor Swarm for Tumor Photothermal Therapy. *Appl. Mater. Today* **2022**, 26, 101348.

(19) Hu, Y.; Liu, W.; Sun, Y. Multiwavelength Phototactic Micromotor with Controllable Swarming Motion for "Chemistry-on-the-Fly." *ACS Appl. Mater. Interfaces* **2020**, 12 (37), 41495-41505.

(20) Liu, H.; Zhang, J.; Jia, Y.; Liu, X.; Chen, X.; Zhao, W.; Mao, C. Theranostic Nanomotors for Tumor Multimode Imaging and Photothermal/Photodynamic Synergistic Therapy. *Chem. Eng. J*. **2022**, 442, 135994.

(21) He, W.; Frueh, J.; Hu, N.; Liu, L.; Gai, M.; He, Q. Guidable Thermophoretic Janus Micromotors Containing Gold Nanocolorifiers for Infrared Laser Assisted Tissue Welding. *Adv. Sci*. 2**016**, 3 (12), 1600206.

(22) Wang, W.; Wu, Z.; Lin, X.; Si, T.; He, Q. Gold-Nanoshell-Functionalized Polymer Nanoswimmer for Photomechanical Poration of Single-Cell Membrane. *J. Am. Chem. Soc*. **2019**, 141 (16), 6601-6608.

(23) Wu, Z.; Lin, X.; Wu, Y.; Si, T.; Sun, J.; He, Q. Near-Infrared Light-Triggered "on/off" Motion of Polymer Multilayer Rockets. *ACS Nano* **2014**, 8 (6), 6097-6105.

(24) Xuan, M.; Mestre, R.; Gao, C.; Zhou, C.; He, Q.; Sánchez, S. Noncontinuous Super-Diffusive Dynamics of a Light-Activated Nanobottle Motor. *Angew. Chem. Int. Ed*. **2018**, 57 (23), 6838-6842.

(25) Ibele, M.; Mallouk, T. E.; Sen, A. Schooling Behavior of Light-Powered Autonomous Micromotors in Water. *Angew. Chem. Int. Ed*. **2009**, 48 (18), 3308-3312.

(26) Wang, X.; Baraban, L.; Misko, V. R.; Nori, F.; Huang, T.; Cuniberti, G.; Fassbender, J.; Makarov, D. Visible Light Actuated Efficient Exclusion between Plasmonic Ag/AgCl Micromotors and Passive Beads. *Small* **2018**, 14 (44), e1802537.

(27) Wang, X.; Baraban, L.; Nguyen, A.; Ge, J.; Misko, V. R.; Tempere, J.; Nori, F.; Formanek, P.; Huang, T.; Cuniberti, G.; Fassbender, J.; Makarov, D. High-Motility Visible Light-Driven Ag/AgCl Janus Micromotors. *Small* **2018**, 14 (48), e1803613.

(28) Zhou, C.; Zhang, H. P.; Tang, J.; Wang, W. Photochemically Powered AgCl Janus Micromotors as a Model System to Understand Ionic Self-Diffusiophoresis. *Langmuir* **2018**, 34 (10), 3289-3295.

(29) Kong, L.; Mayorga-Martinez, C. C.; Guan, J.; Pumper, M. Photocatalytic Micromotors Activated by UV to Visible Light for Environmental Remediation, Micropumps, Reversible Assembly, Transportation, and Biomimicry. *Small* **2020**, 16 (27), e1903179.

(30) Villa, K.; Pumera, M. Fuel-Free Light-Driven Micro/Nanomachines: Artificial Active Matter Mimicking Nature. *Chem. Soc. Rev*. **2019**, 48 (19), 4966-4978.

(31) Eskandarloo, H.; Kierulf, A.; Abbaspourrad, A. Light-Harvesting Synthetic Nano- and Micromotors: A Review. *Nanoscale* **2017**, 9 (34), 12218-12230.

(32) Palagi, S.; Singh, D. P.; Fischer, P. Light-controlled Micromotors and Soft Microrobots. *Adv. Opt. Mater*. **2019**, 7 (16), 1900370.

(33) Šípová-Jungová, H.; Andrén, D.; Jones, S.; Käll, M. Nanoscale Inorganic Motors Driven by Light: Principles, Realizations, and Opportunities. *Chem. Rev*. **2020**, 120 (1), 269-287.

(34) Zhou, D.; Zhuang, R.; Chang, X.; Li, L. Enhanced Light-Harvesting Efficiency and Adaptation: A Review on Visible-Light-Driven Micro/Nanomotors. *Research* **2020**, 6821595.

(35) Dong, R.; Hu, Y.; Wu, Y.; Gao, W.; Ren, B.; Wang, Q.; Cai, Y. Visible-Light-Driven BiOI-Based Janus Micromotor in Pure Water. *J. Am. Chem. Soc*. **2017**, 139 (5), 1722-1725.

(36) Dong, R.; Zhang, Q.; Gao, W.; Pei, A.; Ren, B. Highly Efficient Light-Driven TiO_2-Au Janus Micromotors. *ACS Nano* **2016**, 10 (1), 839-844.

(37) Jang, B.; Hong, A.; Kang, H. E.; Alcantara, C.; Charreyron, S.; Mushtaq, F.; Pellicer, E.; Büchel, R.; Sort, J.; Lee, S. S.; Nelson, B. J.; Pané, S. Multiwavelength Light-Responsive Au/B-TiO_2 Janus Micromotors. *ACS Nano* **2017**, 11 (6), 6146-6154.

(38) Hong, Y.; Diaz, M.; Córdova-Figueroa, U. M.; Sen, A. Light-Driven Titanium-Dioxide-Based Reversible Microfireworks and Micromotor/Micropump Systems. *Adv. Funct. Mater*. **2010**, 20 (10), 1568–1576.

(39) Hong, Y.; Diaz, M.; Córdova-Figueroa, U. M.; Sen, A. Light-Driven Titanium-Dioxide-Based ReversibKochergin, Y. S.; Villa, K.; Novotný, F.; Plutnar, J.; Bojdys, M. J.; Pumera, M. Multifunctional Visible-light Powered Micromotors Based on Semiconducting Sulfur-and Nitrogen-containing Donor-Acceptor Polymer. *Adv. Funct. Mater*. **2020**, 30 (38), 2002701.

(40) Wu, Y.; Si, T.; Shao, J.; Wu, Z.; He, Q. Near-Infrared Light-Driven Janus Capsule Motors: Fabrication, Propulsion, and Simulation. *Nano Res*. **2016**, 9 (12), 3747-3756.

(41) Wu, Z.; Si, T.; Gao, W.; Lin, X.; Wang, J.; He, Q. Superfast Near-Infrared Light-Driven Polymer Multilayer Rockets. *Small* **2016**, 12 (5), 577-582.

(42) Cao, S.; Shao, J.; Wu, H.; Song, S.; De Martino, M. T.; Pijpers, I. A. B.; Friedrich, H.; Abdelmohsen, L. K. E. A.; Williams, D. S.; van Hest, J. C. M. Photoactivated Nanomotors via Aggregation Induced Emission for Enhanced Phototherapy. *Nat. Commun*. **2021**, 12 (1), 2077.

(43) Okawa, D.; Pastine, S. J.; Zettl, A.; Fréchet, J. M. J. Surface Tension Mediated Conversion of Light to Work. *J. Am. Chem. Soc*. **2009**, 131 (15), 5396-5398.

(44) Wang, Y.; Sun, J.; Liao, W.; Yang, Z. Liquid Crystal Elastomer Twist Fibers toward Rotating Microengines. *Adv. Mater*. **2022**, 34 (9), e2107840.

(45) Wang, J.; Xiong, Z.; Tang, J. The Encoding of Light-driven Micro/Nanorobots: From Single to Swarming Systems. *Advanced Intelligent Systems* **2021**, 3 (4), 2000170.

(46) Deng, Z.; Mou, F.; Tang, S.; Xu, L.; Luo, M.; Guan, J. Swarming and Collective Migration of Micromotors under near Infrared Light. *Appl. Mater. Today* **2018**, 13, 45-53.

(47) Dai, B.; Wang, J.; Xiong, Z.; Zhan, X.; Dai, W.; Li, C.-C.; Feng, S.-P.; Tang, J. Programmable Artificial Phototactic Microswimmer. *Nat. Nanotechnol*. **2016**, 11 (12), 1087-1092.

(48) Mou, F.; Zhang, J.; Wu, Z.; Du, S.; Zhang, Z.; Xu, L.; Guan, J. Phototactic Flocking of Photochemical Micromotors. *iScience* **2019**, 19, 415-424.

(49) Zhang, J.; Song, J.; Mou, F.; Guan, J.; Sen, A. Titania-Based Micro/Nanomotors: Design Principles, Biomimetic Collective Behavior, and Applications. *Trends in Chemistry* **2021**, 3 (5), 387-401.

(50) Maric, T.; Nasir, M. Z. M.; Webster, R. D.; Pumera, M. Tailoring Metal/TiO_2 Interface to Influence Motion of Light‐activated Janus Micromotors. *Adv. Funct. Mater*. **2020**, 30 (9), 1908614.

(51) Urso, M.; Ussia, M.; Novotný, F.; Pumera, M. Trapping and Detecting Nanoplastics by MXene-Derived Oxide Microrobots. *Nat. Commun*. **2022**, 13 (1), 3573.

(52) Yuan, K.; de la Asunción-Nadal, V.; Jurado-Sánchez, B.; Escarpa, A. 2D Nanomaterials Wrapped Janus Micromotors with Built-in Multiengines for Bubble, Magnetic, and Light Driven Propulsion. *Chem. Mater*. **2020**, 32 (5), 1983-1992.

(53) Wu, Y.; Boymelgreen, A.; Yossifon, G. Micromotor-Mediated Label-Free Cargo Manipulation. *Curr. Opin. Colloid Interface Sci*. **2022**, 61, 101611.

(54) Zhang, D.; Ren, Y.; Barbot, A.; Seichepine, F.; Lo, B.; Ma, Z.-C.; Yang, G.-Z. Fabrication and Optical Manipulation of Micro-Robots for Biomedical Applications. *Matter* **2022**, 5 (10), 3135-3160.

(55) Villa, K.; Novotný, F.; Zelenka, J.; Browne, M. P.; Ruml, T.; Pumera, M. Visible-Light-Driven Single-Component $BiVO_4$ Micromotors with the Autonomous Ability for Capturing Microorganisms. ACS Nano 2019, 13 (7), 8135–8145.

(56) Li, X.; Wu, R.; Chen, H.; Li, T.; Jiang, H.; Xu, X.; Tang, X.; Wan, M.; Mao, C.; Shi, D. Near-Infrared Light-Driven Multifunctional Tubular Micromotors for Treatment of Atherosclerosis. *ACS Appl. Mater. Interfaces* **2021**, 13 (26), 30930-30940.

(57) Wan, M.; Wang, Q.; Li, X.; Xu, B.; Fang, D.; Li, T.; Yu, Y.; Fang, L.; Wang, Y.; Wang, M.; Wang, F.; Mao, C.; Shen, J.; Wei, J. Systematic Research and Evaluation Models of Nanomotors for Cancer Combined Therapy. *Angew. Chem. Int. Ed*. **2020**, 59 (34), 14458-14465.

(58) Wu, T.; Nieminen, T. A.; Mohanty, S.; Miotke, J.; Meyer, R. L.; Rubinsztein-Dunlop, H.; Berns, M. W. A Photon-Driven Micromotor Can Direct Nerve Fibre Growth. *Nat. Photonics* **2012**, 6 (1), 62-67.

Chapter 2

Light-driven Nanomotors Boosted by Single-atom Catalysis

2.1 Introduction

Emerging catalytic nano/micromotors powered by biocompatible and environmental friendly fuel sources offer considerable promise for diverse biomedical and environmental applications [1-5]. Light, one of the best external stimuli to drive the motion of nano/micromotors, has been widely employed to design powerful photocatalytic nano/micromotors [6-10]. However, the application of most reported photocatalytic nano/micromotors is commonly limited to the use of toxic chemical fuels (such as H_2O_2 or N_2H_4). Therefore, efforts have been devoted to developing fuel-free light-driven nano/micromotors for efficient operation in pure water [11-18]. Currently, light-driven nano/micromotors are largely limited to slow motion speeds and triggered light with specific wavelengths, especially in pure water without the presence of chemical fuels. This is mainly because of the fast electron-hole recombination, resulting in a lower efficiency of photocatalytic generation of asymmetric gradients, which dramatically limits the performance, especially the speed and power, of the photocatalytic nano/micromotors. TiO_2, as one of the most classical and widely used photocatalysts, has shown significant merits in fabricating light-driven nano/micromotors, including desired motion speed, wireless photocontrollablility, chemical stability, low cost, photodegradation capability and multi-wavelength response [11-15, 19-26]. To date, titania-based nano/micromotors have exhibited considerable potential in applications such as environment remediation, sensing and cargo delivery [27]. Of the various types of titania-based nano/micromotors, TiO_2 Janus nano/micromotors are commonly used due to the simple fabrication process and excellent motion behaviors. Pt Sputtering technique is often applied to TiO_2 microspheres to fabricate microscale TiO_2 Janus motors, and the role of sputtered metals as a coating layer has been clarified [28]. Further improvements are desired to enhance the efficiency, power and capabilities of such light-powered TiO_2 Janus nano/micromotors. Identifying excellent photocatalysts as active particles is crucial for designing efficient light-driven nano/micromotors. Single-atom catalysts have recently emerged as promising candidates for high-performance photocatalysts owing to the obvious

advantages of maximum atom utilization efficiency and outstanding catalytic activity [29-33]. In addition, as photocatalysts of heterogeneous reactions, such as the hydrogen evolution reaction, TiO_2-supported single-atom catalysts have an advantage over conventional TiO_2-based photocatalysts because of their improved durability and reversibility with enhanced efficiency [34-42].

2.2 Experimental Methods

2.2.1 Material Synthesis and Characterization

All the starting materials were obtained from Sigma-Aldrich. Commercially available reagents were used without further purification unless noted otherwise. All other chemicals were reagent grade or better. Ultrapure water was obtained from Invitrogen.

2.2.1.1 Preparation of single-atom Cu/TiO_2-Pt Janus Nanomotors

First, single-atom Cu/TiO_2 hollow nanospherical photocatalysts were synthesized based on a previously reported wrap-bake-peel process [34]. 10 μg single-atom Cu/TiO_2 photocatalysts were first dispersed in 150 μL ethanol. The sample was then spread onto glass slides and dried uniformly to form particle monolayers. Then, the Pt (other metals: Au, Cu) layer was sputtered on Cu/TiO_2 nanospherical photocatalysts with a Denton Discovery 18 system at room temperature. The Pt (other metals: Au, Cu) layer was deposited with an output power of 200 W for 200 s. The micromotors were subsequently released from the glass slides via pipette pumping and dispersed into ultrapure water.

2.2.1.2 Preparation of Cu/TiO_2 reference-Pt and TiO_2 Reference-Pt Nanomotors

To fabricate the Cu/TiO_2 reference, the synthesis was performed in the same manner as for the previous section, but without using SiO_2 as a template or coating layer. First, TiO_2 was formed by a hydrolysis reaction, followed by Cu ion adsorption onto the TiO_2 surface and annealing at 900 °C for 2h in air. To fabricate the TiO_2 reference, the synthesis was performed in the same manner as Cu/TiO_2 reference but without Cu doping.

2.2.1.3 Labeling of Nanomotors

The as-prepared Janus nanomotors were further labeled by graphene quantum dots using a previously reported method [44].

2.2.1.4 TEM Characterization

TEM images were taken by Thermofisher Talos F200X microscope operated at 200 kV. The nanoscale EDS mapping was conducted using 4 in-column SDD Super-X windowless detectors with 10 kcps output under STEM mode.

2.2.1.5 Atomic-resolution Imaging on Cs-corrected STEM.

Atomic-resolution imaging of Rh/TiO_2 was conducted on the double spherical aberration-corrected JEOL JEM-ARM300CF (Japan) operating under 300 kV. All atomic-resolutions images were generated on a high-angle annular dark-field detector (HAADF) with an inner collection angle ~ 80 mrad. The point-to-point response is 0.83 Å.

2.2.1.6 X-ray absorption Spectroscopy Measurements and Data Processing

XAFS spectra of the Cu K-edge were collected at the XAFS for the catalysis beamline of the Singapore Synchrotron Light Source (SSLS), Singapore. The acquired EXAFS data were extracted and processed according to the standard procedures using the ATHENA module implemented in the IFEFFIT software packages to obtain the EXAFS spectra and the wavelet transform contour plot.

Table 1. EXAFS fitting parameters at the Cu K-edge（S_0^2=0.87）

Sample	Path	C.N.	R (Å)	$\sigma^2\times10^3$ (Å^2)	ΔE (eV)	R factor
Cu	Cu-O	4	1.96 ± 0.01	8.4 ± 1.3	-0.6 ± 1.0	0.011
	Cu-Ti	6	2.92 ± 0.05	27.8 ± 2.7	-13.4 ± 4.7	

2.2.2 Motion Behavior Measurement and Calibration Experiments

Total internal reflection fluorescence (TIRF) microscopy at UC San Diego Nikon Imaging Center was applied to study the motion behavior and calibration experiments of fluorescent-labeled single-atom

Cu/TiO_2-Pt Janus nanomotors. The microscope was equipped with a LU-NV laser launch (Nikon), with 405nm, 488nm, 532nm, 561nm, and 640nm laser lines. The 488nm and 405nm laser channels were selected to illuminate the photocatalytic nanomotors as the light source. The power density (Table 1) of the 488nm laser channel is tunable from 0-40mW/cm^2. Illumination, video and image acquisition, and calibration experiments were controlled and performed by NIS Elements Advanced Research software (Nikon).

Table 2. The power density of 488nm and 405nm laser channels of TIRF microscopy

	25%	30%	40%	50%	75%	100%
488nm	4.82mW/cm^2	6.74 mW/cm^2	10mW/cm^2	16.1mW/cm^2	29mW/cm^2	40mW/cm^2
405nm	0.438mW/cm^2	0.608mW/cm^2	1.02mW/cm^2	1.505mW/cm^2	2.67mW/cm^2	3.58mW/cm^2

2.2.3 Statistical Analysis of Motion Behavior

All the motion behavior analysis were performed by NIS Elements Advanced Research software, ImageJ, and Matlab.

2.2.4 Electrochemical Potential Measurements

Tafel plots are used to obtain the potential of each nanomotor part (Pt, Au, Cu, and single-atom Cu/TiO_2) in an ultrapure water environment. Pt, Au, Cu electrodes, and single-atom Cu/TiO_2 films on glass electrodes were used as the working electrode in the electrochemical potential measurements, respectively. We use the Autolab PGSTAT204 potentiostat/galvanostat to test the potential at a scan rate of 5 mV/s and over a potential range of -0.3 to 0.6 V (vs Ag/AgCl, 3 M KCl reference) along with a Pt counter electrode.

2.2.5 Photocatalytic Degradation Experiments

Photodegradation activities of single-atom Cu/TiO_2-Pt Janus nanomotors and two control groups were evaluated by the degradation of Methylene blue, Rhodamine B, Methyl orange under 488nm light

irradiation (40 mW·cm^{-2}). In a typical process, 250 μL nanomotor suspensions were added to 10mL 10μM dye solutions. Before photodegradation reactions, the various mixtures were stirred without illumination for 1h to achieve a dynamic chemical equilibrium. Afterward, the various mixtures were irradiated with 488nm light (40 mW·cm^{-2}). The samples were then divided into various aliquots and abstracted at the desired time intervals. The photodegradation efficiency and kinetics for the three dye pollutants of the single-atom Cu/TiO_2-Pt Janus nanomotors are further evaluated by measuring UV-Vis spectrophotometry (Biotek, United States).

2.2.6 DLS Size Distribution

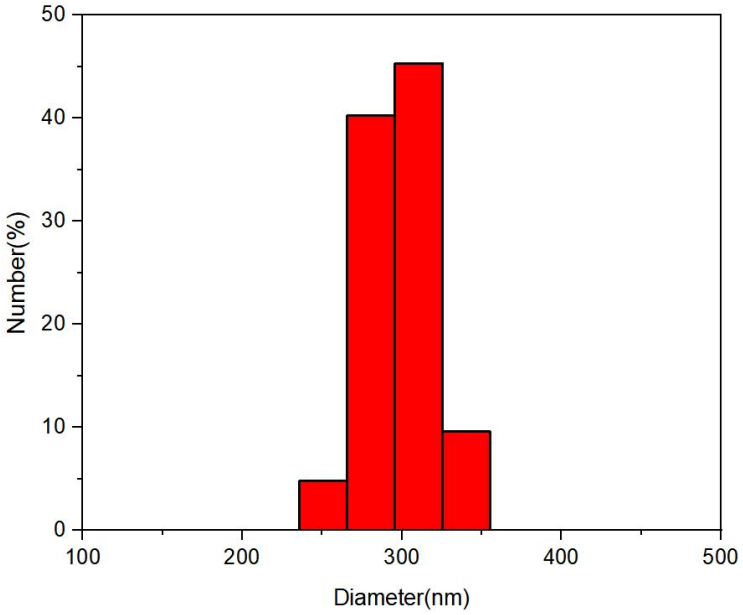

Figure 2.1. The DLS size distribution of Janus single-atom Cu/TiO_2-Pt nanomotors

2.3 Results and Discussion

Herein, we present highly efficient visible-light powered Janus Cu SAs/TiO_2-Pt nanomotors (~ 300nm in diameter) based on a Cu SAs/TiO_2 hollow nanosphere photocatalyst for effective operation in pure water. The photocatalytic process (Figure 2.2A) is activated by the change of the valence states of Cu sites that occupied the most stable Ti vacancies, thus converting the adjacent TiO_2 in the resting state to active [34]. This mechanism by doping single-atom Cu into TiO_2 tremendously improves the efficiency of photoexcited charge separation and transport, leading to a remarkable self-electrophoretic effect to

drive the ultrafast movement of the nanomotors. The Janus Cu SAs/TiO_2-Pt nanomotors rely on the light-driven self-electrophoresis mechanism and exhibit a very fast speed (average speed: 23 μm/s, around 75 body length/s) under a 40 mW/cm^2 intensity of visible light in the fuel-free pure water environment.

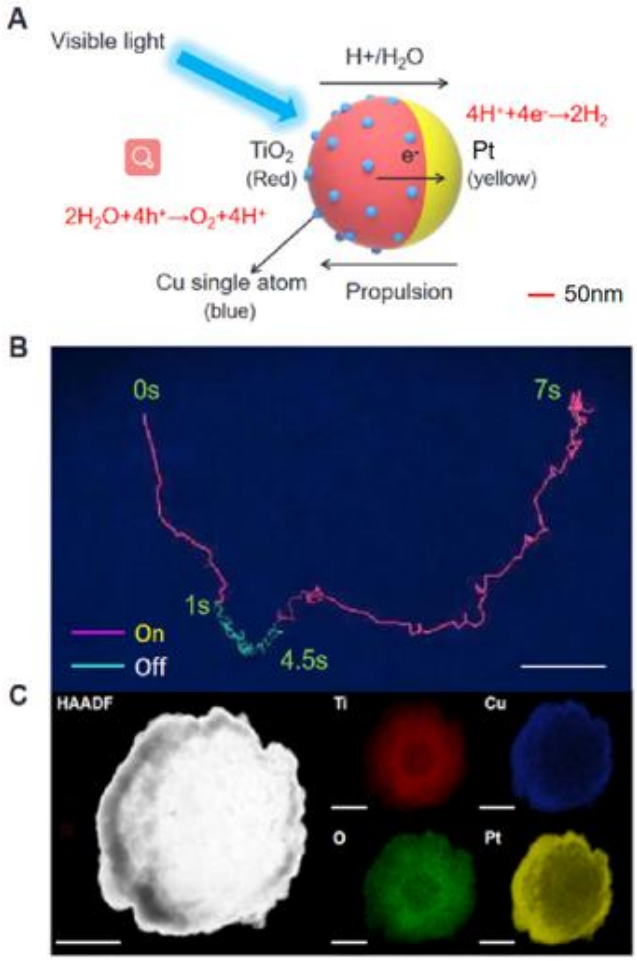

Figure 2.2. (A) Schematic of Janus Cu SAs/TiO_2-Pt nanomotors powered by visible light in water. (B) Time-lapse images illustrate "On" and "Off" UV light activation of the Janus Cu SAs/TiO_2-Pt nanomotor. Scale bar, 10 μm. (C) HAADF-STEM image of a spherical Janus Cu SAs/TiO_2-Pt nanomotor and the corresponding energy-dispersive X-ray spectroscopy (EDS) elemental map images for Ti, O, Cu, and Pt, respectively. Scale bar, 100 nm.

Since the propulsion of Janus Cu SAs/TiO_2-Pt nanomotors is controlled by "on" and "off" switching of visible light, they move extremely fast directionally when the light is "on" due to the self-electrophoretic effect. On the contrary, only very weak local motion is observed upon switching the light "off" (Figure 2.2B). The dramatic speed enhancement, compared to corresponding Janus Cu

nanoparticles/TiO_2 nanomotors, could be attributed to the cooperative photoactivation of Cu SAs/TiO_2 photocatalysts and the hollow spherical structure of Janus Cu SAs/TiO_2-Pt nanomotors. The single-atom catalysis in this process is facilitated primarily by the electronic band structure of Cu single-atoms and their interaction with hollow TiO_2 nanosphere supports. The fabricated Janus Cu SAs/TiO_2 nanomotors are first characterized by HAADF-STEM and EDS (Figure 2.2C). The thicker layer, as shown in the nanomotor STEM image and Pt EDS image, verifies the formation of the Janus structure. As distinct from existing light-powered motors, we report on the first applications of single-atom catalysis to design efficient nano/micromotors. The as-prepared single-atom nanomotors display an ultrafast speed (average speed: 23 μm/s) in pure water with a small submicron size (~ 300 nm in diameter), i.e., 75 body-length/sec, and offer excellent photocatalytic degradation capability.

To validate the presence of single atoms in the Ti vacancies of hollow TiO_2 nanomotors, we performed aberration-corrected HAADF-STEM studies on the Rh/TiO_2 due to the sharper contrast of Rh atoms on the TiO_2 support compared to Cu [34]. The red circled bright spots are single Rh atoms (Figure 2.3A). In X-ray absorption near-edge structure (XANES) spectroscopy, the valence of Cu species in Cu/TiO_2 is much close to +2 (Cu^{2+} will be completely reduced to Cu^{+} during the photoactivation process) while compared to the reference samples, and also shows typical characteristics of Cu^{2+} absorption edge energy around 8997 eV (Figure 2.3B). The k^3-weighted Fourier transform extended X-ray absorption fine structure (FT-EXAFS) spectra in Figure 2.3C show the Cu/TiO_2 own peaks at ~ 1.5 Å and at ~2.4 Å, which correspond to the Cu-O first coordination shell and Cu-Ti backscattering. Additionally, no Cu-Cu bond is found. R-space fitting and the corresponding wavelet transform (WT) analysis further confirmed the successful preparation of Cu SAs/TiO_2 photocatalyst (Figure 2.3D and 2.3E) [34].

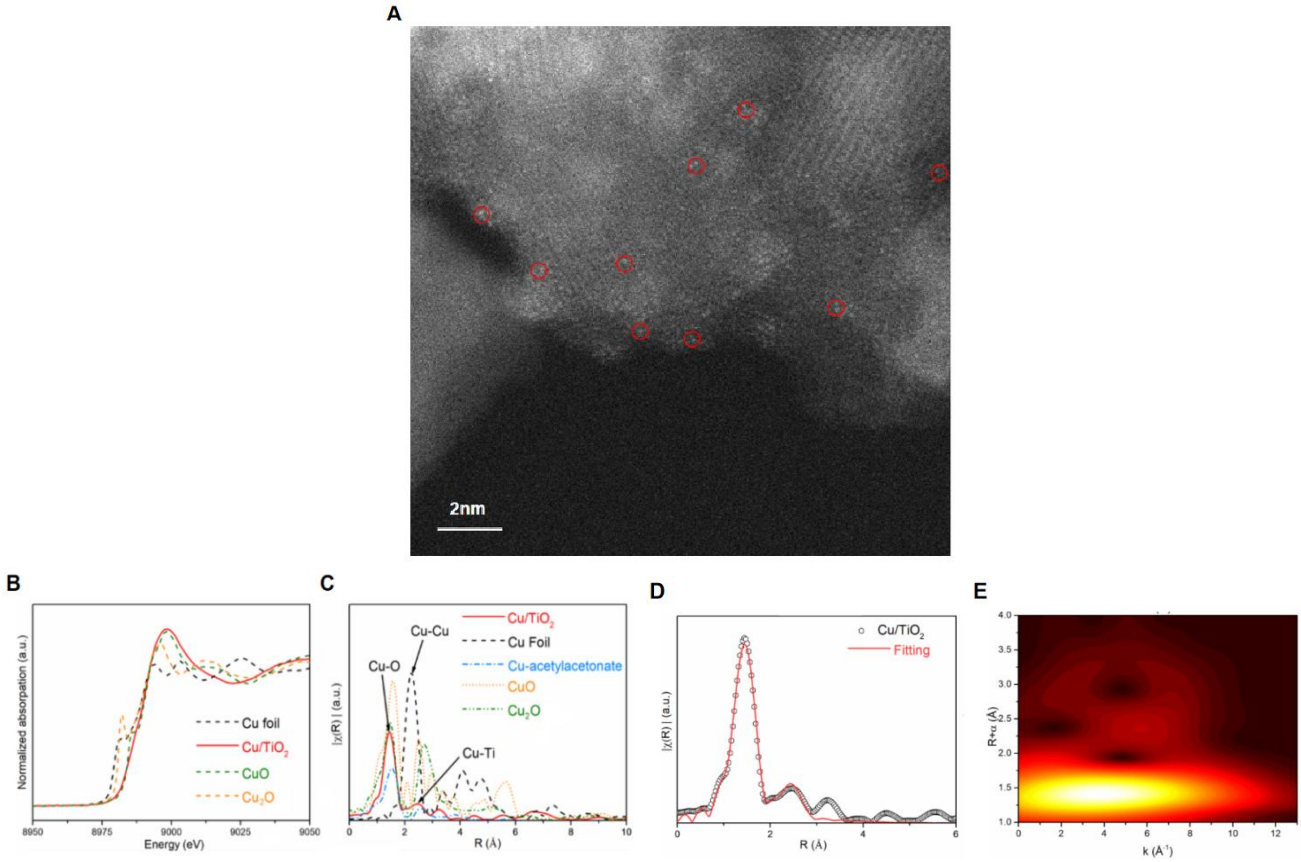

Figure 2.3 (A) Atomic-resolution Cs-corrected STEM HAADF images of single-atom Rh/TiO_2. (B) XANES, (C) FT-EXAFS, and (D) EXAFS fitting spectra, and (E) WT analysis of Cu SAs/TiO_2 at Cu K-edges.

The motion behaviour of such Janus Cu SAs/TiO_2-Pt nanomotors has been further demonstrated. To confirm the increased activity caused by single-atom sites, the motion performance of Janus Cu SAs/TiO_2-Pt nanomotors is compared to two control groups with a similar method but without the formation of Cu single atoms: Janus Cu nanoparticles/TiO_2-Pt nanomotors (Cu NPs/TiO_2 reference-Pt) and Janus TiO_2-Pt nanomotors (TiO_2 reference-Pt). Cu NPs/TiO_2 reference TiO_2 reference were prepared without calcination and doping steps. The test environment is achieved by illuminating them with blue light (488 nm) at an intensity of 40 mW·cm^{-2} in pure water. Under this condition, the mean speed of the Janus Cu SAs/TiO_2-Pt nanomotors is 23.0 ± 3.5 μm/s which is significantly higher than the speed of Cu/TiO_2 reference-Pt 1.9 ± 0.5 μm/s and TiO_2 Reference-Pt nanomotors 0.8 ± 0.2 μm/s (Figure 2.4B). Figure 3D examines the effect of light intensity on the speed of Janus Cu SAs/TiO_2-Pt nanomotors. These data clearly indicate that the speed increases rapidly upon increasing the light intensity from 2.5 mW/cm^2 to 40 mW/cm^2. In addition, the mean squared displacement (MSD) is

calculated for three different types of nanomotors (Figure 2.4A) and various light intensities (Figure 2.4C). The MSD curves further establish the change from Brownian motion to directional movement upon incorporating the single-atom catalysis and increasing the light intensity. Figure 2.4E illustrates the significant difference in tracking trajectories between the nanomotors and the other two control groups. To track the movement with a total internal reflection fluorescence (TIRF) microscopy, the nanomotors were labeled with graphene quantum dots using a previously reported method. The Janus Cu SAs/TiO_2-Pt nanomotor can move at a speed of over 20 μm/s, corresponding to a relative speed of more than 50 body lengths/s. In stark contrast to the nanomotors facilitated by single-atom catalysis (Figure 2.4E i), the propulsion of the other two control groups (Figure 2.4E ii) is quite slow over 15s.

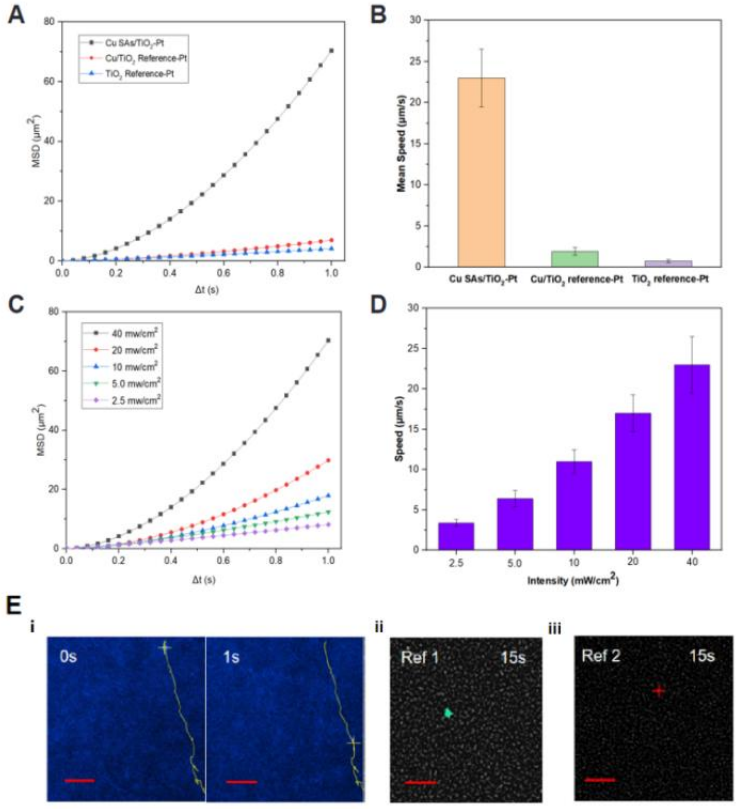

Figure 2.4 (A) 2D mean square displacement (MSD) experimental data for the Cu SAs/TiO_2-Pt, Cu NPs/TiO_2 reference-Pt and TiO_2 reference-Pt nanomotors in water (N = 20). (B) Average (N = 10) mean speed of the Cu SAs/TiO_2-Pt, Cu NPs/TiO_2 reference-Pt and TiO_2 reference-Pt nanomotors in water at 488-nm-light irradiation (40 mW·cm^{-2}). (C) MSD data for the Cu SAs/TiO_2-Pt nanomotors with different intensities of light in water (N = 20). (D) Effect of visible light intensity on the motor speed in water (N = 10). (E) Trajectories of (i) Cu SAs/TiO_2-Pt Janus nanomotors over 1s (ii) Cu NPs/TiO_2 reference-Pt nanomotors (Ref 1) over 15s (iii) TiO_2 reference-Pt nanomotors (Ref 2) over 15s. Scale bar: 5 μm.

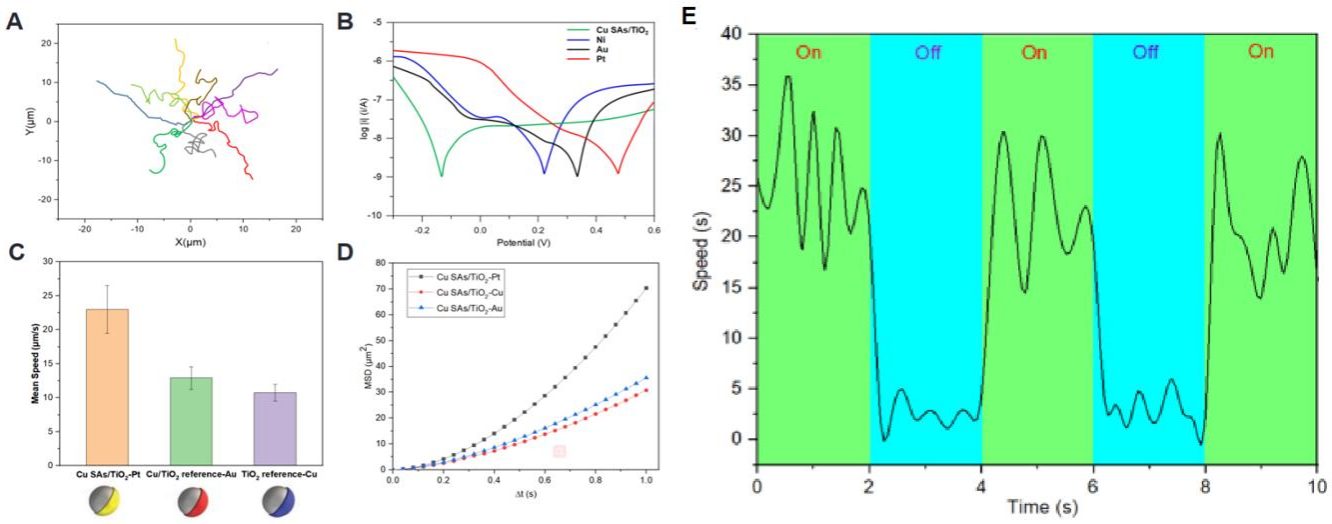

Figure 2.5 (A) Trajectory of 10 nanomotors in aqueous solution with X- and Y-coordinates under 488-nm-light irradiation (40 mW·cm^{-2}) for 1s. (B) Tafel plot of Pt, Au, Ni and Cu SAs/TiO_2 with illumination. (C) Average (N = 10) mean speed of the Cu SAs/TiO_2-Pt, Cu SAs/TiO_2-Au, Cu SAs/TiO_2-Cu nanomotors in water at 488-nm-light irradiation (40 mW·cm^{-2}). (D) MSD data for the Cu SAs/TiO_2-Pt, Cu SAs/TiO_2-Au, Cu SAs/TiO_2-Cu nanomotors in water (N = 20). (E) Corresponding speed/time dependence illustrating the UV light triggered "On/Off" motion control of the Cu SAs/TiO_2-Pt Janus nanomotors in pure water without any additional chemicals. (Light intensity: 40 mW·cm^{-2}).

Analysis of the XY trajectories indicates a universally directional fast movement of nanomotors (Figure 2.5A). To further explain the impact of sputtered metal in fabricating Janus nanomotors, the mixed potentials of Cu SAs/TiO_2 with illumination and different metal electrodes (e.g., Au, Pt) have been examined (Figure 2.5B). It is apparent that the potential difference of Cu SAs/TiO_2-Pt (621 mV) is much larger than that of Cu SAs/TiO_2-Au (474 mV). This is consistent with the motion behavior (speed and MSD) of the nanomotors displayed in Figures 2.5C and 2.5D. The mean speed of the Janus Cu SAs/TiO_2-Pt nanomotors is 23.0 ± 3.5 μm/s, which is substantially higher than the speed of the Janus Cu SAs/TiO_2-Au (12.9 ± 1.7 μm/s) and Janus Cu SAs/TiO_2-Cu nanomotors (10.8 ± 1.2 μm/s).

In many biomedical and environmental applications of nano/micromotors, switchable movement is always of particular interest. Light-driven nano/micromotors have distinct merit in this aspect. The nanomotors move fast when the light is turned on and display only a slow random Brownian motion upon switching the light off (Figure 2.5E). Such repetitive on/off motion behavior reflects the highly reversible and light-controllable "stop/go" property of the nanomotors.

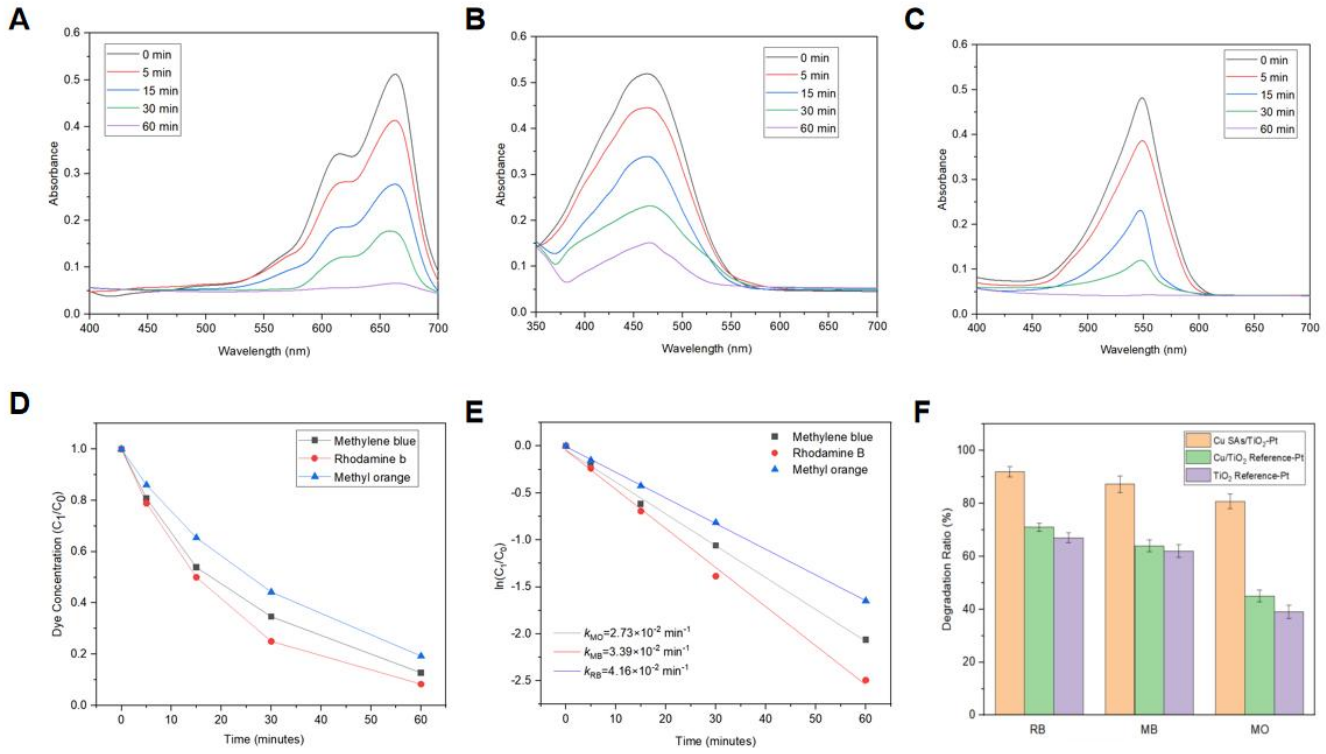

Figure 2.6 (A-C) UV–vis spectra of 10 μM aqueous solutions of three different dyes (Methylene blue (A), Rhodamine B (B), and Methyl orange (C)) during different degradation times in the presence of nanomotors under 488-nm-light irradiation (40 mW·cm^{-2}). (D) Kinetics of degradation of three different dyes. (E) Photodegradation rates of three different dyes. (F) Photodegradation efficiencies of three different dyes in the presence of Cu SAs/TiO_2-Pt, Cu NPs/TiO_2 reference-Pt and TiO_2 reference-Pt nanomotors in aqueous solutions.

Environmental remediation is one of the most important applications of photocatalytic nano/micromotors [45-46]. Since in the dye solutions, the self-electrophoresis-based propulsion of nanomotors will be tremendously enhanced [13], we systematically investigate the photodegradation capability of the new nanomotors towards three common dyes (Methylene blue, Rhodamine B, Methyl orange). The dye degradation efficiency can be quantitatively evaluated by the decreased absorption intensity of their UV-Vis spectra. We measured the spectra of three dyes in 10 μM aqueous solution over 60 minutes under treatment (Figure 2.6A-C). The remarkable reduction of dye solutions containing nanomotors through visible light irradiation over 60 minutes indicates significant degradation of the dyes. Then, we investigated the kinetics of such photodegradation of three dyes in the presence of nanomotors. As shown in Figure 2.6D, the extent of degradation of Methylene blue, Rhodamine B, and Methyl orange in 60min is 80.77%, 87.31%, 91.73%, respectively, confirming the attractive

photodegradation capability of the nanomotors. Then, the photodegradation rates have been further calculated (Figure 2.6E). These data show that the degradation reactions of three dyes follow the first-order reaction kinetics. The corresponding photodegradation reaction rate constants of three dyes are 2.73×10^{-2} min^{-1} (Methyl orange), 3.39×10^{-2} min^{-1} (Methylene blue), 3.39×10^{-2} min^{-1} (Rhodamine B). Moreover, we compare these three dyes in the presence of Janus Cu SAs/TiO_2-Pt, Cu NPs/TiO_2 reference-Pt and TiO_2 reference-Pt nanomotors to further explore the effect of the nanomotors in photodegradation (Figure 2.6F). It is clear that the degradation efficiencies of the three dyes in the presence of Cu SAs/TiO_2-Pt nanomotors are significantly higher than those observed for the other two control groups. These findings clearly illustrate that the enhanced propulsion of nanomotors driven by single-atom photocatalysis improves the photodegradation performance of dyes.

2.4 Conclusions

To the best of our knowledge, the research related to light-driven titania-based nanomotors operating in pure water is still rare compared to microscale motors. The development of such nanoscale motors faces various challenges and opportunities [47-49]. In this work, we developed and demonstrated Janus Cu SAs/TiO_2-Pt nanomotors facilitated by single-atom catalysis, which exhibit an outstanding motion behavior in pure water when illuminated by visible light. Such capabilities have not been realized by previously reported light-powered nano/micromotors and greatly overcome the current limitations and challenges: (1) The motion speeds in pure water without the addition of chemical fuels are slow; (2) The light-powered Janus nanomotors are still rarely reported, and their performance still needs to be improved especially in pure water and under visible light illumination. The nanomotors show enhanced speeds upon increasing the light intensity and possess “stop-go” control driven by “on” and “off” of the light. Moreover, it was found that the photodegradation performance of such single atom nanomotors is remarkably better than that of control groups. Our pioneering introduction of single-atom catalysis into designing catalytic nano/micromotors paves the way for future studies. These findings thus provide

valuable insights and inspiration for designing and fabricating high-performance light-driven nanomotors that have tremendous potential for environmental and biomedical applications.

2.5 References

(1) J.Wang, Nanomachines: fundamentals and applications, Wiley, Hoboken, 2013.

(2) Guix, M.; Mayorga-Martinez, C. C.; Merkoçi, A. Nano/Micromotors in (Bio)Chemical Science Applications. *Chem. Rev*. **2014**, 114 (12), 6285-6322.

(3) Sánchez, S.; Soler, L.; Katuri, J. Chemically Powered Micro- and Nanomotors. *Angew. Chem. Int. Ed*. **2015**, 54 (5), 1414-1444.

(4) Wang, H.; Pumera, M. Fabrication of Micro/Nanoscale Motors. *Chem. Rev*. **2015**, 115 (16), 8704-8735.

(5) Safdar, M.; Khan, S. U.; Jänis, J. Progress toward Catalytic Micro- and Nanomotors for Biomedical and Environmental Applications. *Adv. Mater*. **2018**, 30 (24), e1703660.

(6) Xu, L.; Mou, F.; Gong, H.; Luo, M.; Guan, J. Light-Driven Micro/Nanomotors: From Fundamentals to Applications. *Chem. Soc. Rev*. **2017**, 46 (22), 6905-6926.

(7) Wang, J.; Xiong, Z.; Zheng, J.; Zhan, X.; Tang, J. Light-Driven Micro/Nanomotor for Promising Biomedical Tools: Principle, Challenge, and Prospect. *Acc. Chem. Res*. **2018**, 51 (9), 1957-1965.

(8) Zhou, D.; Zhuang, R.; Chang, X.; Li, L. Enhanced Light-Harvesting Efficiency and Adaptation: A Review on Visible-Light-Driven Micro/Nanomotors. *Research*. 2020, 6821595.

(9) Safdar, M.; Simmchen, J.; Jänis, J. Light-Driven Micro- and Nanomotors for Environmental Remediation. *Environ. Sci. Nano* **2017**, 4 (8), 1602-1616.

(10) Villa, K.; Pumera, M. Fuel-Free Light-Driven Micro/Nanomachines: Artificial Active Matter Mimicking Nature. *Chem. Soc. Rev*. **2019**, 48 (19), 4966-4978.

(11) Dong, R.; Zhang, Q.; Gao, W.; Pei, A.; Ren, B. Highly Efficient Light-Driven TiO_2-Au Janus Micromotors. *ACS Nano* **2016**, 10 (1), 839-844.

(12) Sridhar, V.; Park, B.-W.; Sitti, M. Light-Driven Janus Hollow Mesoporous TiO_2-Au Microswimmers. *Adv. Funct. Mater*. **2018**, 28 (25), 1704902.

(13) Wu, Y.; Dong, R.; Zhang, Q.; Ren, B. Dye-Enhanced Self-Electrophoretic Propulsion of Light-Driven TiO_2-Au Janus Micromotors. *Nano-micro Lett*. **2017**, 9 (3), 30.

(14) Wang, X.; Sridhar, V.; Guo, S.; Talebi, N.; Miguel-López, A.; Hahn, K.; van Aken, P. A.; Sánchez,

S. Fuel-Free Nanocap-like Motors Actuated under Visible Light. *Adv. Funct. Mater*. **2018**, 28 (25), 1705862.

(15) Dong, R.; Hu, Y.; Wu, Y.; Gao, W.; Ren, B.; Wang, Q.; Cai, Y. Visible-Light-Driven BiOI-Based Janus Micromotor in Pure Water. *J. Am. Chem. Soc*. **2017**, 139 (5), 1722-1725.

(16) Liu, W.; Chen, X.; Ding, X.; Long, Q.; Lu, X.; Wang, Q.; Gu, Z. Visible-Light-Driven Cuprous Oxide Nanomotors with Surface-Heterojunction-Induced Propulsion. *Nanoscale Horiz* **2021**, 6 (3), 238-244.

(17) Wang, Q.; Dong, R.; Yang, Q.; Wang, J.; Xu, S.; Cai, Y. Highly Efficient Visible-Light-Driven Oxygen-Vacancy-Based $Cu_{2+1}O$ Micromotors with Biocompatible Fuels. *Nanoscale Horiz* **2020**, 5 (2), 325-330.

(18) Villa, K.; Novotný, F.; Zelenka, J.; Browne, M. P.; Ruml, T.; Pumera, M. Visible-Light-Driven Single-Component $BiVO_4$ Micromotors with the Autonomous Ability for Capturing Microorganisms. *ACS Nano* **2019**, 13 (7), 8135-8145.

(19) Dai, B.; Wang, J.; Xiong, Z.; Zhan, X.; Dai, W.; Li, C.-C.; Feng, S.-P.; Tang, J. Programmable Artificial Phototactic Microswimmer. *Nat. Nanotechnol*. **2016**, 11 (12), 1087-1092.

(20) Tang, S.; Zhang, F.; Zhao, J.; Talaat, W.; Soto, F.; Karshalev, E.; Chen, C.; Hu, Z.; Lu, X.; Li, J.; Lin, Z.; Dong, H.; Zhang, X.; Nourhani, A.; Wang, J. Structure-dependent Optical Modulation of Propulsion and Collective Behavior of Acoustic/Light-driven Hybrid Microbowls. *Adv. Funct. Mater*. **2019**, 29 (23), 1809003.

(21) Chen, C.; Tang, S.; Teymourian, H.; Karshalev, E.; Zhang, F.; Li, J.; Mou, F.; Liang, Y.; Guan, J.; Wang, J. Chemical/Light-Powered Hybrid Micromotors with "On-the-Fly" Optical Brakes. *Angew. Chem., Int. Ed*. **2018**, 57, 8110−8114.

(22) Li, J.; Liu, W.; Wang, J.; Rozen, I.; He, S.; Chen, C.; Kim, H. G.; Lee, H.-J.; Lee, H.-B.-R.; Kwon, S.-H.; Li, T.; Li, L.; Wang, J.; Mei, Y. Nanoconfined Atomic Layer Deposition of TiO_2/Pt Nanotubes: Toward Ultrasmall Highly Efficient Catalytic Nanorockets. *Adv. Funct. Mater*. **2017**, 27 (24), 1700598.

(23) Kong, L.; Mayorga-Martinez, C. C.; Guan, J.; Pumera, M. Fuel-Free Light-Powered TiO_2/Pt Janus Micromotors for Enhanced Nitroaromatic Explosives Degradation. *ACS Appl. Mater. Interfaces* **2018**, 10 (26), 22427-22434.

(24) Kong, L.; Ambrosi, A.; Nasir, M. Z. M.; Guan, J.; Pumera, M. Self-propelled 3D-printed "Aircraft Carrier" of Light-powered Smart Micromachines for Large-volume Nitroaromatic Explosives Removal. *Adv. Funct. Mater*. **2019**, 29 (39), 1903872.

(25) Jang, B.; Hong, A.; Kang, H. E.; Alcantara, C.; Charreyron, S.; Mushtaq, F.; Pellicer, E.; Büchel, R.; Sort, J.; Lee, S. S.; Nelson, B. J.; Pané, S. Multiwavelength Light-Responsive Au/B-TiO_2 Janus Micromotors. *ACS Nano* **2017**, 11 (6), 6146-6154.

(26) Sridhar, V.; Park, B.-W.; Guo, S.; van Aken, P. A.; Sitti, M. Multiwavelength-Steerable Visible-Light-Driven Magnetic CoO-TiO_2 Microswimmers. *ACS Appl. Mater. Interfaces* **2020**, 12 (21), 24149-24155.

(27) Zhang, J.; Song, J.; Mou, F.; Guan, J.; Sen, A. Titania-Based Micro/Nanomotors: Design Principles, Biomimetic Collective Behavior, and Applications. *Trends in Chemistry* **2021**, 3, 387-401.

(28) Maric, T.; Nasir, M. Z. M.; Webster, R. D.; Pumera, M. Tailoring Metal/TiO_2 Interface to Influence Motion of Light-activated Janus Micromotors. *Adv. Funct. Mater*. **2020**, 30 (9), 1908614.

(29) Xue, Z.-H.; Luan, D.; Zhang, H.; (David) Lou, X. W. Single-Atom Catalysts for Photocatalytic Energy Conversion. *Joule* **2022**, 6 (1), 92-133.

(30) Xia, Y.; Sayed, M.; Zhang, L.; Cheng, B.; Yu, J. Single-Atom Heterogeneous Photocatalysts. *Chem Catalysis* **2021**, 1 (6), 1173-1214.

(31) Gao, C.; Low, J.; Long, R.; Kong, T.; Zhu, J.; Xiong, Y. Heterogeneous Single-Atom Photocatalysts: Fundamentals and Applications. *Chem. Rev*. **2020**, 120 (21), 12175-12216.

(32) Ji, S.; Chen, Y.; Wang, X.; Zhang, Z.; Wang, D.; Li, Y. Chemical Synthesis of Single Atomic Site Catalysts. *Chem. Rev*. **2020**, 120 (21), 11900-11955.

(33) Guo, W.; Wang, Z.; Wang, X.; Wu, Y. General Design Concept for Single-Atom Catalysts toward Heterogeneous Catalysis. *Adv. Mater*. **2021**, 33 (34), e2004287.

(34) Lee, B.-H.; Park, S.; Kim, M.; Sinha, A. K.; Lee, S. C.; Jung, E.; Chang, W. J.; Lee, K.-S.; Kim, J. H.; Cho, S.-P.; Kim, H.; Nam, K. T.; Hyeon, T. Reversible and Cooperative Photoactivation of Single-Atom Cu/TiO_2 Photocatalysts. *Nat. Mater*. **2019**, 18 (6), 620-626.

(35) Chen, Y. J.; Ji, S. F.; Sun, W. M.; Lei, Y. P.; Wang, Q. C.; Li, A.; Chen, W. X.; Zhou, G.; Zhang, Z. D.; Wang, Y.; Zheng, L. R.; Zhang, Q. H.; Gu, L.; Han, X. D.; Wang, D. S.; Li, Y. D. Engineering the Atomic Interface with Single Platinum Atoms for Enhanced Photocatalytic Hydrogen Production. *Angew. Chem., Int. Ed*. **2020**, 59, 1295-1301.

(36) Yi, D.; Lu, F.; Zhang, F.; Liu, S.; Zhou, B.; Gao, D.; Wang, X.; Yao, J. Regulating Charge Transfer of Lattice Oxygen in Single-Atom Doped Titania for Hydrogen Evolution. *Angew. Chem., Int. Ed*. **2020**, 59, 15855-15859.

(37) Xiao, M.; Zhang, L.; Luo, B.; Lyu, M.; Wang, Z.; Huang, H.; Wang, S.; Du, A.; Wang, L. Molten-Salt-Mediated Synthesis of an Atomic Nickel Co-catalyst on TiO_2 for Improved Photocatalytic H_2 Evolution. *Angew. Chem., Int. Ed*. **2020**, 59, 7230-7234.

(38) Zhang, W.; He, H.; Li, H.; Duan, L.; Zu, L.; Zhai, Y.; Li, W.; Wang, L.; Fu, H.; Zhao, D. Visible-light Responsive TiO_2-based Materials for Efficient Solar Energy Utilization. *Adv. Energy*

Mater. **2020**, 2003303.

(39) Cheng, C.; Fang, W.-H.; Long, R.; Prezhdo, O. V. Water Splitting with a Single-Atom Cu/TiO_2 Photocatalyst: Atomistic Origin of High Efficiency and Proposed Enhancement by Spin Selection. *JACS Au* **2021**, 1 (5), 550-559.

(40) Xi, J.; Zhang, X.; Zhou, X.; Wu, X.; Wang, S.; Yu, W.; Yan, N.; Loh, K. P.; Xu, Q.-H. Titanium Dioxide Hierarchical Microspheres Decorated with Atomically Dispersed Platinum as an Efficient Photocatalyst for Hydrogen Evolution. *J. Colloid Interface Sci*. **2022**, 623, 799-807.

(41) Zhang, Y.; Zhao, J.; Wang, H.; Xiao, B.; Zhang, W.; Zhao, X.; Lv, T.; Thangamuthu, M.; Zhang, J.; Guo, Y.; Ma, J.; Lin, L.; Tang, J.; Huang, R.; Liu, Q. Single-Atom Cu Anchored Catalysts for Photocatalytic Renewable H_2 Production with a Quantum Efficiency of 56. *Nat. Commun*. **2022**, 13 (1), 58.

(42) Li, D.; Zhao, Y.; Zhou, C.; Zhang, L.-P.; Tang, J.; Zhang, T. Unveiling the Critical Role of TiO_2-Supported Atomically Dispersed Cu Species for Enhanced Photofixation of N_2 to Nitrate. *Fundamental Research* **2022**.

(43) Gu, F.; Qin, X.; Li, M.; Xu, Y.; Hong, S.; Ouyang, M.; Giannakakis, G.; Cao, S.; Peng, M.; Xie, J.; Wang, M.; Han, D.; Xiao, D.; Wang, X.; Wang, Z.; Ma, D. Selective Catalytic Oxidation of Methane to Methanol in Aqueous Medium over Copper Cations Promoted by Atomically Dispersed Rhodium on TiO_2. *Angew. Chem. Int. Ed*. **2022**, 61 (18), e202201540.

(44) Li, H.; He, X.; Kang, Z.; Huang, H.; Liu, Y.; Liu, J.; Lian, S.; Tsang, C. H. A.; Yang, X.; Lee, S. T. Water-Soluble Fluorescent Carbon Quantum Dots and Photocatalyst Design. *Angew. Chem., Int. Ed*. **2010**, 49, 4430-4434.

(45) Kong, L.; Mayorga-Martinez, C. C.; Guan, J.; Pumera, M. Photocatalytic Micromotors Activated by UV to Visible Light for Environmental Remediation, Micropumps, Reversible Assembly, Transportation, and Biomimicry. *Small* **2020**, 16 (27), e1903179.

(46) Parmar, J.; Vilela, D.; Villa, K.; Wang, J.; Sánchez, S. Micro- and Nanomotors as Active Environmental Microcleaners and Sensors. *J. Am. Chem. Soc*. **2018**, 140 (30), 9317-9331.

(47) Šípová-Jungová, H.; Andrén, D.; Jones, S.; Käll, M. Nanoscale Inorganic Motors Driven by Light: Principles, Realizations, and Opportunities. *Chem. Rev*. **2020**, 120 (1), 269-287.

(48) Wang, W.; Mallouk, T. E. A Practical Guide to Analyzing and Reporting the Movement of Nanoscale Swimmers. *ACS Nano* **2021**, 15 (10), 15446-15460.

(49) Novotný, F.; Wang, H.; Pumera, M. Nanorobots: Machines Squeezed between Molecular Motors and Micromotors. *Chem* **2020**, 6 (4), 867-884.

Chapter 3

Light-driven $SrTiO_3$:Al-based Nanomotors for Antimicrobial Applications

3.1 Introduction

Photocatalytic nano/micromotors that can convert light energy into ultrafast locomotion are a topic of particular interest with huge potential in antimicrobial applications, environmental remediation, sensing, and drug delivery [1-7]. So far, various light-powered nano/micromotors based on semiconductor oxide photocatalysts have been reported, including TiO_2, ZnO, BiOI, $BiVO_4$, Cu_2O, WO_3, Fe_2O_3, Bi_2WO_6 (perovskite-like structure), etc [8-19]. However, to the best of our knowledge, nano/micromotors based on ABO_3 perovskite structure have never been studied.

$SrTiO_3$, one of the most promising photocatalysts, has exhibited superior catalytic performance. Recently, Domen reported an excellent $SrTiO_3$:Al catalyst after modification with a quantum efficiency as high as 96% in the ultraviolet band (350-360 nm) [20]. The catalyst solves the problem of electron-hole recombination by increasing the crystallinity and reducing lattice defects. In addition, the introduction of cocatalysts improves the efficiency of hydrogen and oxygen generation and avoids the occurrence of side reactions [21].

Photocatalytic materials with free radicals generated, ions released or plasmonic effect under illumination have exhibited huge potential for rapidly inactivating bacteria and viruses [22-23]. Among these, $SrTiO_3$ has shown exceptional performance and been widely used [24-28].

Recently, photocatalytic nano/micromotors for antimicrobial applications have developed rapidly due to their superior performance and efficiency [3, 29-35]. Here, we demonstrate a light-driven nanoswimmer based on a Janus STO:Al-Au structure. Ag nanoparticles are further deposited on the nanoswimmers to gift the outstanding antibacterial capability and enhanced motion performance of nanoswimmers with plasmonic effect [36-39]. The Janus STO:Al-Au/Ag nanoswimmers show excellent motion speeds in pure water (28μm/s under the illumination of 40mW/cm^2 UV light) and various biological media. The nanoswimmers are applied to the active and efficient disinfection of *Escherichia coli* (*E. coli*), which is also facilitated by the characteristic of fast movement of the nanoswimmers.

3.2 Experimental Methods

3.2.1 Fabrication of Janus STO:Al-Au/Ag nanoswimmers.

STO:Al photocatalysts were fabricated according to previously reported methods [20] and characterized by transmission electron microscopy (TEM) (Figure 3.1).

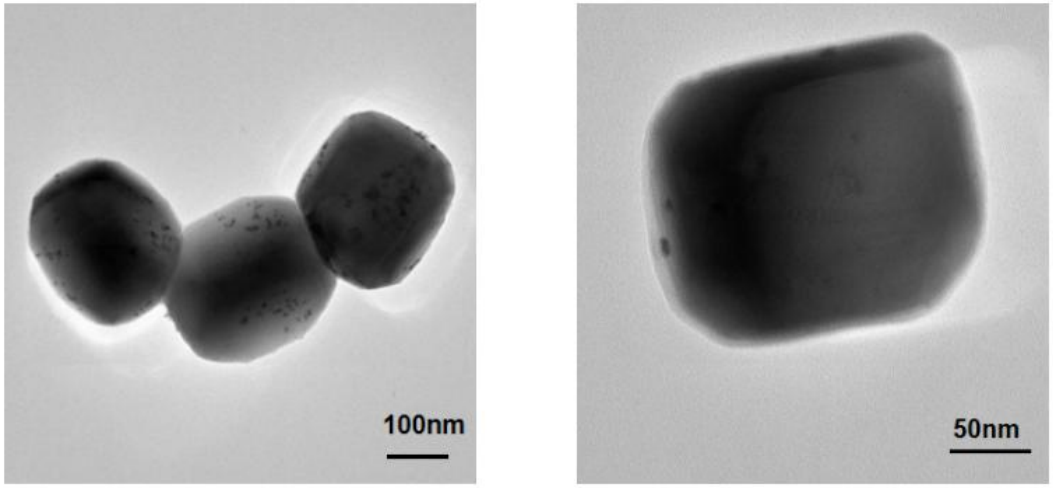

Figure 3.1 TEM images of $SrTiO_3$:Al

The monolayer of STO:Al was prepared on clean glass slides. The slides were exposed to oxygen plasma for 10 min to make the surface hydrophilic. 100 μL of ethanol suspension containing STO:Al was dropped onto the glass slides. Janus STO/Au nanostructures were fabricated by Au sputtering on half side of the STO:Al nanoparticles with a thickness of 30 nm. The formed Janus STO/Au were collected by sonication in deionized water and centrifugation. Ag NPs (5nm) were synthesized via a modified chemical reduction method [40]. 1 mL $AgNO_3$ (0.2 M) and 0.5 g poly(N-vinyl-2-pyrrolidone) (PVP, MW ≈ 55000) were added to a round-bottom flask which contained 15 mL of deionized water. The mixture was stirred for 30 min, then $NaBH_4$ (0.1 M) solution was added slowly until Ag^+ was fully reduced. The as-prepared Ag NPs were redispersed in ultrapure water at a concentration of approximately 5 mg/mL. Previously fabricated Janus STO/Au nanostructures were incubated with a 1 mM cysteamine hydrochloride solution in ethanol overnight. The nanoparticles were washed with ethanol and incubated for 12 hours with a diluted solution of the previously prepared AgNPs in ethanol. Afterwards, the incubated solution was sonicated for 30 min, and the fabricated Janus STO:Al-Au/Ag

nanoswimmers were washed twice. The nanomotors were stored in ethanol. Before experiments, they were washed and redispersed in fresh ultrapure water.

3.2.2 Motion Behaviors of Janus STO:Al-Au/Ag nanoswimmers.

The as-prepared Janus STO:Al-Au/Ag nanoswimmers were further labeled by nitrogen-doped graphene quantum dots (NGQDs) based on a modified method reported previously [41]. 300 mg graphene quantum dots powder was dispersed in 50 mL aqueous ammonia solution and by ultrasonic treatment for 1 hour. Then, the solution was added to a 100 mL Teflon-lined stainless steel autoclave and reacted at 160℃ overnight. The obtained sample was purified and lyophilized for further use. 5% NGQDs aqueous solution was prepared and added to the aqueous solution Janus STO:Al-Au/Ag nanoswimmers. The mixture was stirred at 90℃ for 1 hour, dried at 60 ℃ overnight in a vacuum oven, and resuspended in the aqueous solution.

Total internal reflection fluorescence (TIRF) microscopy was applied to study the motion behavior and calibration experiments of fluorescent-labeled Janus STO:Al-Au/Ag nanoswimmers. The 405 nm and 488 nm laser channels were selected to illuminate the nanomotors as the light source. A UV light source was applied to irradiate the nanomotors with various power densities. Illumination, video and image acquisition, and calibration experiments were controlled and performed by NIS Elements Advanced Research software (Nikon).

3.2.3 COMSOL Simulation.

The surrounding fluid of the nanoswimmer is modeled as an incompressible Newtonian fluid. Since Reynold number is approaching zero given the small characteristics dimensions and velocity of the nano-swimmer, Stokes equations can be used to describe the fluid motion:

$$\mu\nabla^2\boldsymbol{u} = \boldsymbol{\nabla}p \ \ , \ \boldsymbol{\nabla}\cdot\boldsymbol{u} = 0$$

where p is pressure and u is velocity, μ is dynamic viscosity. Electroosmotic slip from Helmholtz-Smoluchowski relation is used as the boundary condition for Stokes equations:

$$u_{bc} = -\frac{\epsilon\zeta}{\mu}E_t$$

where ζ is zeta potential at the surface and ϵ is the permittivity of the fluid, and E_t is the tangential electric field at the outer EDL boundary which needs to be computed by solving the electrostatic potential distribution. The electrostatics was modeled using the Laplace equation assuming electroneutral of the bulk solution and the charge separation only happened inside the EDL region:

$$\nabla^2\phi = 0$$

Where ϕ is the electrical potential. The anode of our swimmer produces H^+, and the cathode consumes H^+, at a constant rate which determined the normal electric field at the anode and cathode surface. The ion transport process inside the EDL was encapsulated using the following analytical expression derived through perturbation analysis, which assumed a steady state balance between diffusive and migratory ion flux density:

$$-\frac{\partial\phi}{\partial n} = E_n = \frac{J_{H^+}k_bT}{2eD_{H^+}n_\infty}$$

Where E_n is the normal electric field pointing out of the EDL outer boundary, J_{H^+} is the hydrogen flux at the surface, $\frac{k_bT}{e}$ is the thermal voltage, $D_{H^+}$is diffusivity and $n_\infty$is the bulk concentration of H^+.

3.2.4 Assessments of In Vitro Antibacterial Activity.

E. coli was cultured overnight in Luria–Bertani broth in a rotatory shaker and refreshed with the medium at a 1:100 dilution. Bacteria were obtained by centrifuging and washed with phosphate buffer saline (10 mM, pH = 7.4). All the bacteria were initially diluted to an optical density value of 0.3 at 600 nm. To study the antimicrobial activity of STO:Al-based nanomotors, the bacteria of OD_{600} = 0.3 were washed with pure water three times and further diluted. Then equivalent nanomotors were respectively dispersed in the diluted bacteria. After being incubated for 60min, the viability of bacteria was determined by counting the number of colonies formed.

3.3 Results and Discussion

As illustrated in Figure 1a, Janus STO:Al-Au/Ag nanoswimmers were fabricated through Au sputtering on $SrTiO_3$:Al to obtain asymmetric structure followed by Ag nanoparticles deposition. HAADF-STEM-EDS analysis confirms the successful preparation of Janus STO:Al-Au/Ag nanoswimmers (Figure 1b).

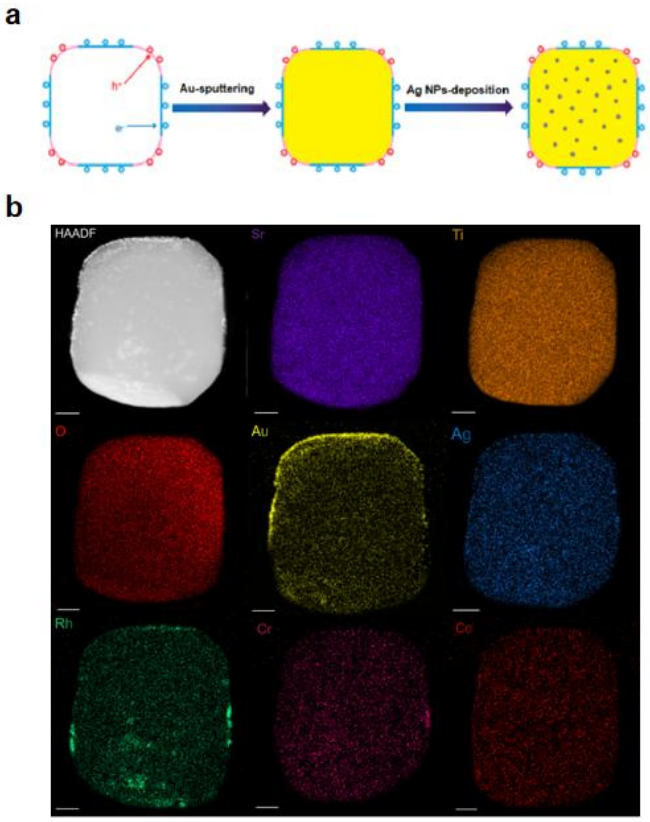

Figure 3.2 (a) Schematic of the multi-step fabrication procedure of Janus STO:Al-Au/Ag nanoswimmers (b) HAADF-STEM image of Janus STO:Al-Au nanoswimmers and the corresponding energy-dispersive X-ray spectroscopy (EDS) elemental map images. Scale bar, 250 nm

The photocatalytic processes taking place on the nanoswimmer surface under light illumination are schematically shown in Figure 3.2a. Protons are produced from the oxidation of water at STO:Al and the generated electrons are consumed during the reduction of protons at Au layer. The OER and HER co-catalysts are alternately distributed on the sides of the octagon which further improves the photocatalytic performance of the nanoswimmer. Such mechanism synergistically facilitates the ultrafast movement of the nanoswimmer. To explore the enhanced performance of the nanoswimmer caused by plasmonic effect, the electromagnetic field distribution is analyzed by finite difference time domain (FDTD) simulation method [36, 42-43]. Figures 3.2b gives the calculated electronic field

distributions of under the illumination of UV light with λ = 365 nm. The mapping indicates the ratio of the intensity of the plasmonic field to that of the excitation light. It is seen that the plasmonic field is generated with maximal intensities occur at the interface between STO:Al and gold layer deposited with silver nanoparticles. Figures 3.2c further verifies the plasmonic effect of the nanoswimmers. The emerging peak (450-600 nm) of UV-Vis adsorption spectra originated from the localized surface plasmonic resonance effect of Ag NPs and Au layer [38, 44-46].

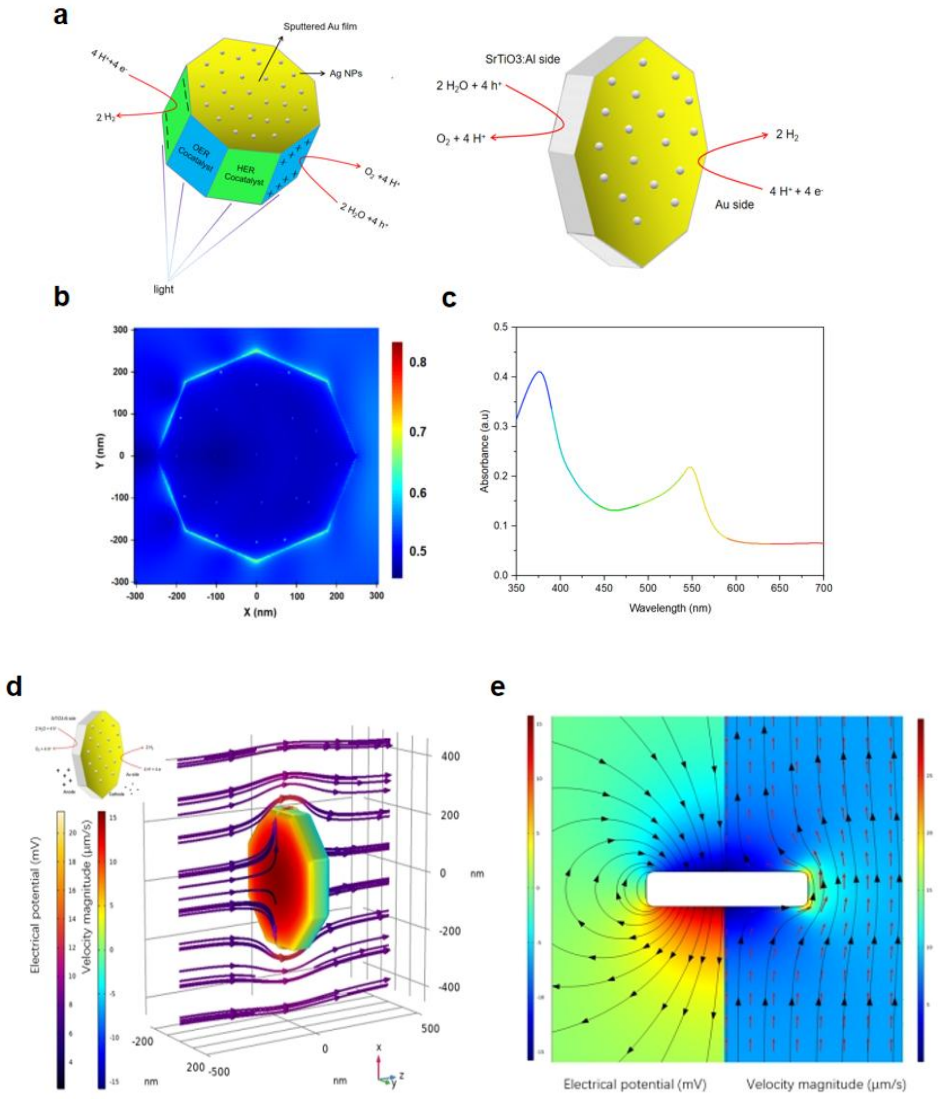

Figure 3.3 (a) Scheme illustrating the excitation process and propulsion mechanism of the Janus STO:Al-Au/Ag nanoswimmers. (b) Simulated plasmonic electric field distribution (normal-z direction) of the Janus STO:Al-Au/Ag nanoswimmer under the excitation of 365 nm. (c) UV-Vis absorption spectra and of the Janus STO:Al-Au/Ag nanoswimmers. (d) Surface plot of electrical potential profiles, and velocity streamlines colored by velocity magnitude Left side: Anode ($SrTiO_3$:Al); Right side: Cathode (Au). (e) Left: 2D slice (0, y, z plane) of the 3D electrical potential profile. Right: 2D slice (0, y, z plane) of the 3D flow profile.

The motion behaviour of such Janus STO:Al-Au/Ag nanoswimmers in various conditions has been further explored. As shown in Figure 3.3a, the motion speeds of Janus STO:Al-Au/Ag, Janus STO:Al-Au and STO:Al/Ag were tested under illumination of UV light, 405nm and 488nm visible light (40mW/cm^2). The ranking of speed has the following trends: (1) Janus STO:Al-Au/Ag > Janus STO:Al-Au > STO:Al/Ag (2) UV > 405nm > 488nm. Such results match the optical and structural properties of the nanoswimmers. To further verify the outstanding motion performance of the nanoswimmer, we select PS nanosphere with the same size (500nm) as the control group for comparison (Figure 3b). The trajectories indicate that the Janus STO:Al-Au/Ag moves very fast directionally while the PS inert particle does not show effective movement. Figure 3c investigates the impact of UV light intensity on the speed of Janus STO:Al-Au/Ag nanoswimmers, which demonstrates the speed increases significantly upon increasing the light intensity from 5 mW/cm^2 to 40 mW/cm^2. The mean squared displacement (MSD) is calculated for three different types of nanoswimmers (Figure 3.3d). The MSD curves further establish Janus STO:Al-Au/Ag and Janus STO:Al-Au nanoswimmers can move directionally under UV illumination. However, Janus STO:Al-Au/Ag nanoswimmers without UV illumination and Ag NPs-STO under UV illumination only show weak brownian motion. This reveals the necessity of the existence of Janus structures and light to lead to ultrafast and efficient movement. Analysis of the XY trajectories as a function of time indicates a universally directional ultrafast movement of nanoswimmers (Figure 3.3e). To evaluate the motion performance of the nanoswimmers in various biological media, the speeds of the nanoswimmers in pure water, 1×PBS, LB media under 40 mW/cm^2 UV illumination are tested (Figure 3.3f). Although the motion speeds are significantly reduced due to the high concentration of ions, it is still desirably fast, which ensures the effective movement of nanoswimmers under high salt concentration for more environmental and biomedical applications [47].

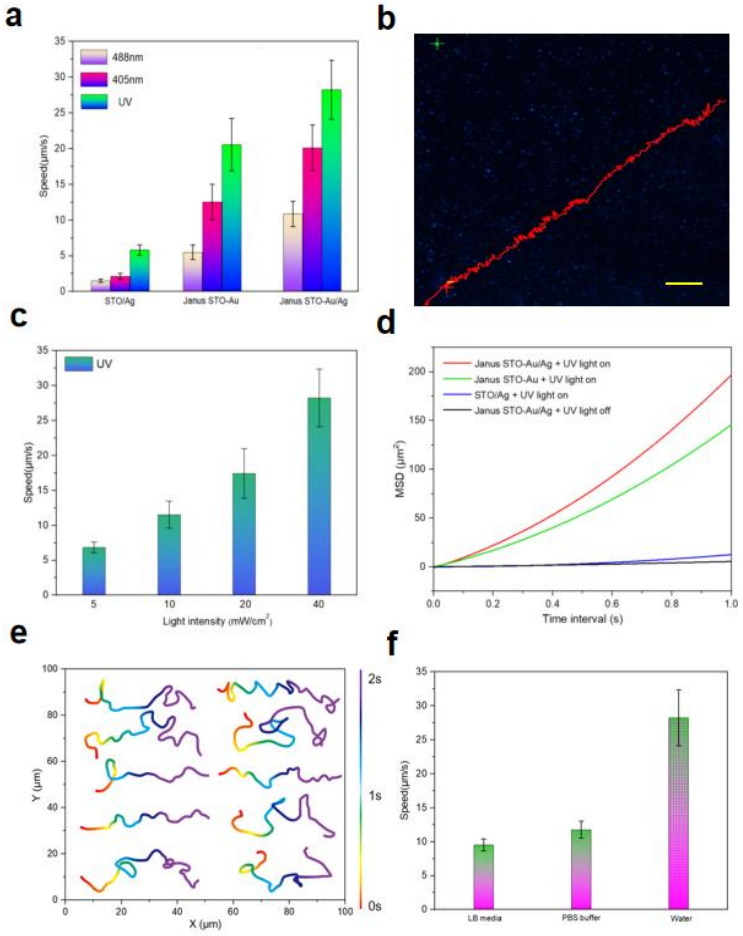

Figure 3.4 (a) Mean speeds (N = 10) of Ag NPs-STO, Janus STO:Al/Au, Janus STO:Al-Au/Ag nanoswimmers with visible light (405nm, 488nm, 40mW/cm^2) and UV light (40mW/cm^2). (b) Trajectories of the Janus STO:Al-Au/Ag nanoswimmer (red) and 500nm PS nanosphere (green, control group) over 10s. Scale bar: 10μm. (c) Effect of UV light intensity on the nanoswimmer speed in water (N = 10). (d) Average MSD versus time interval (Δt = 1 s) for Janus STO:Al-Au/Ag, Janus STO/Au, Ag NPs-STO nanoswimmers with UV light (40 mW·cm^{-2}) and Ag-NPs-Janus STO/Au without UV light. (e) Trajectory of 10 nanomotors in aqueous solution with X- and Y-coordinates under UV-light irradiation (40 mW·cm^{-2}) for 2s. (f) Mean speeds (N = 10) of Janus STO:Al-Au/Ag nanoswimmers in various biological media (pure water, 1 × PBS, LB media) swimming under UV light illumination.

In addition, the Janus STO-Au/Ag nanoswimmers exhibit outstanding antibacterial performance. Compared to the STO-Au, STO and the negative control group, STO-Au/Ag nanoswimmers kill *E. coli* very effectively (Figure 4a-4b) and furthermore, the better performance with light illuminition over dark verifies the superiority of the light-driven motion of nanoswimmers and plasmonic antibacterial capacity (Figure 4c-4d).

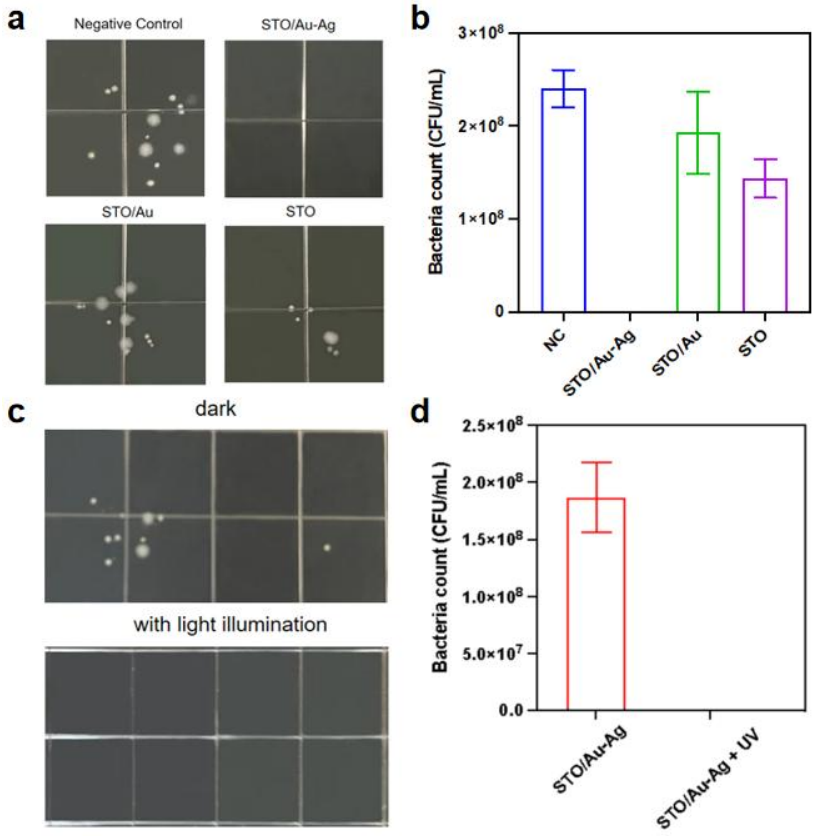

Figure 3.5 The antibacterial activity of the STO nanomotors against *E. coli* bacteria. (a, c) Photographs of bacterial colonies, (b, d) the bacterial viabilities of *E. coli* after different treatments.

3.4 References

(1) Wang, J. *Nanomachines: Fundamentals and Applications*; Wiley-VCH: Weinheim, Germany, 2013.

(2) Parmar, J.; Vilela, D.; Villa, K.; Wang, J.; Sanchez, S. Micro- and Nanomotors as Active Environmental Microcleaners and Sensors. *J. Am. Chem. Soc*. **2018**, 140, 9317−9331.

(3) Zhang, Z.; Wang, L.; Chan, T. K. F.; Chen, Z.; Ip, M.; Chan, P. K. S.; Sung, J. J. Y.; Zhang, L. Micro-/Nanorobots in Antimicrobial Applications: Recent Progress, Challenges, and Opportunities. *Adv. Healthc. Mater*. **2022**, 11 (6), e2101991.

(4) Xu, L.; Mou, F.; Gong, H.; Luo, M.; Guan, J. Light-Driven Micro/Nanomotors: From Fundamentals to Applications. *Chem. Soc. Rev*. **2017**, 46 (22), 6905–6926.

(5) Villa, K.; Pumera, M. Fuel-Free Light-Driven Micro/Nanomachines: Artificial Active Matter Mimicking Nature. *Chem. Soc. Rev*. **2019**, 48 (19), 4966–4978.

(6) Dong, R.; Cai, Y.; Yang, Y.; Gao, W.; Ren, B. Photocatalytic Micro/Nanomotors: From Construction to Applications. *Acc. Chem. Res*. **2018**, 51 (9), 1940–1947.

(7) Jurado-Sánchez, B.; Wang, J. Micromotors for Environmental Applications: A Review. *Environ. Sci. Nano* **2018**, 5 (7), 1530–1544.

(8) Dong, R.; Zhang, Q.; Gao, W.; Pei, A.; Ren, B. Highly Efficient Light-Driven TiO_2-Au Janus Micromotors. *ACS Nano* **2016**, 10 (1), 839–844.

(9) Chen, C.; Mou, F.; Xu, L.; Wang, S.; Guan, J.; Feng, Z.; Wang, Q.; Kong, L.; Li, W.; Wang, J.; Zhang, Q. Light-Steered Isotropic Semiconductor Micromotors. *Adv. Mater*. **2017**, 29 (3), 1603374.

(10) Chen, C.; Tang, S.; Teymourian, H.; Karshalev, E.; Zhang, F.; Li, J.; Mou, F.; Liang, Y.; Guan, J.; Wang, J. Chemical/Light-Powered Hybrid Micromotors with "On-the-Fly" Optical Brakes. *Angew. Chem., Int. Ed*. **2018**, 57, 8110−8114.

(11) Du, S.; Wang, H.; Zhou, C.; Wang, W.; Zhang, Z. Motor and Rotor in One: Light-Active ZnO/Au Twinned Rods of Tunable Motion Modes. *J. Am. Chem. Soc*. **2020**, 142 (5), 2213–2217.

(12) Dong, R.; Hu, Y.; Wu, Y.; Gao, W.; Ren, B.; Wang, Q.; Cai, Y. Visible-Light-Driven BiOI-Based Janus Micromotor in Pure Water. *J. Am. Chem. Soc*. **2017**, 139 (5), 1722–1725.

(13) Heckel, S.; Bilsing, C.; Wittmann, M.; Gemming, T.; Büttner, L.; Czarske, J.; Simmchen, J. Beyond Janus Geometry: Characterization of Flow Fields around Nonspherical Photocatalytic Microswimmers. *Adv. Sci*. **2022**, 9 (24), e2105009.

(14) Villa, K.; Novotný, F.; Zelenka, J.; Browne, M. P.; Ruml, T.; Pumera, M. Visible-Light-Driven Single-Component $BiVO_4$ Micromotors with the Autonomous Ability for Capturing Microorganisms. *ACS Nano* **2019**, 13 (7), 8135–8145.

(15) Liu, W.; Chen, X.; Ding, X.; Long, Q.; Lu, X.; Wang, Q.; Gu, Z. Visible-Light-Driven Cuprous Oxide Nanomotors with Surface-Heterojunction-Induced Propulsion. *Nanoscale Horiz* **2021**, 6 (3), 238–244.

(16) Tan, H.; Chen, B.; Liu, M.; Jiang, J.; Ou, J.; Liu, L.; Wang, F.; Ye, Y.; Gao, J.; Sun, J.; Peng, F.; Tu, Y. Adaptive Cu_2O Micromotors with pH-Responsive Phototaxis Reversal. *Chem. Eng. J*. **2022**, 448,

137689.

(17) Zhang, Q.; Dong, R.; Wu, Y.; Gao, W.; He, Z.; Ren, B. Light-Driven Au-WO_3@C Janus Micromotors for Rapid Photodegradation of Dye Pollutants. *ACS Appl. Mater. Interfaces* **2017**, 9 (5), 4674–4683.

(18) Zhou, D.; Ren, L.; Li, Y. C.; Xu, P.; Gao, Y.; Zhang, G.; Wang, W.; Mallouk, T. E.; Li, L. Visible Light-Driven, Magnetically Steerable Gold/Iron Oxide Nanomotors. *Chem. Commun*. **2017**, 53 (83), 11465–11468.

(19) Villa, K.; Děkanovský, L.; Plutnar, J.; Kosina, J.; Pumera, M. Swarming of Perovskite-like Bi_2WO_6 Microrobots Destroy Textile Fibers under Visible Light. *Adv. Funct. Mater*. **2020**, 30 (51), 2007073.

(20) Takata, T.; Jiang, J.; Sakata, Y.; Nakabayashi, M.; Shibata, N.; Nandal, V.; Seki, K.; Hisatomi, T.; Domen, K. Photocatalytic Water Splitting with a Quantum Efficiency of Almost Unity. *Nature* **2020**, 581 (7809), 411–414.

(21) Moss, B.; Wang, Q.; Butler, K. T.; Grau-Crespo, R.; Selim, S.; Regoutz, A.; Hisatomi, T.; Godin, R.; Payne, D. J.; Kafizas, A.; Domen, K.; Steier, L.; Durrant, J. R. Linking in Situ Charge Accumulation to Electronic Structure in Doped $SrTiO_3$ Reveals Design Principles for Hydrogen-Evolving Photocatalysts. *Nat. Mater*. **2021**, 20 (4), 511–517.

(22) Ganguly, P.; Byrne, C.; Breen, A.; Pillai, S. C. Antimicrobial Activity of Photocatalysts: Fundamentals, Mechanisms, Kinetics and Recent Advances. *Appl. Catal. B* **2018**, 225, 51–75.

(23) Parra-Ortiz, E.; Malmsten, M. Photocatalytic Nanoparticles - From Membrane Interactions to Antimicrobial and Antiviral Effects. *Adv. Colloid Interface Sci*. **2022**, 299, 102526.

(24) Kiss, B.; Manning, T. D.; Hesp, D.; Didier, C.; Taylor, A.; Pickup, D. M.; Chadwick, A. V.; Allison, H. E.; Dhanak, V. R.; Claridge, J. B.; Darwent, J. R.; Rosseinsky, M. J. Nano-Structured Rhodium Doped $SrTiO_3$-Visible Light Activated Photocatalyst for Water Decontamination. *Appl. Catal. B* **2017**, 206, 547–555.

(25) Yamaguchi, Y.; Usuki, S.; Kanai, Y.; Yamatoya, K.; Suzuki, N.; Katsumata, K.-I.; Terashima, C.; Suzuki, T.; Fujishima, A.; Sakai, H.; Kudo, A.; Nakata, K. Selective Inactivation of Bacteriophage in

the Presence of Bacteria by Use of Ground Rh-Doped $SrTiO_3$ Photocatalyst and Visible Light. *ACS Appl. Mater. Interfaces* **2017**, 9 (37), 31393–31400.

(26) Bae, H. S.; Manikandan, V.; Hwang, J. H.; Seo, Y.-S.; Chung, H.-S.; Ryu, H. I.; Chae, W.-S.; Cho, M.; Ekambe, P. S.; Jang, J. S. Photocatalytic Degradation of Organic Pollutants and Inactivation of Pathogens under Visible Light via CoO_x Surface-Modified Rh/Sb-Doped $SrTiO_3$ Nanocube. *J. Mater. Sci*. **2021**, 56 (30), 17235–17253.

(27) Zhang, Y.; Li, Y.; Ruan, Z.; Yuan, Y.; Lin, K. Extensive Solar Light Utilizing by Ternary C-Dots/Cu_2O/$SrTiO_3$: Highly Enhanced Photocatalytic Degradation of Antibiotics and Inactivation of *E. Coli*. *Chemosphere* **2022**, 290, 133340.

(28) Chen, J.; Guo, X.; Lang, L.; Yin, X.; Wang, A.; Rui, Z. Multifunctional Z-Scheme Cu_xO/Ag/$SrTiO_3$ Heterojunction for Photothermocatalytic VOCs Degradation and Antibiosis. *Appl. Surf. Sci*. **2022**, No. 153275.

(29) Ussia, M.; Urso, M.; Dolezelikova, K.; Michalkova, H.; Adam, V.; Pumera, M. Active Light-powered Antibiofilm ZnO Micromotors with Chemically Programmable Properties. *Adv. Funct. Mater*. **2021**, 31 (27), 2101178.

(30) Liu, X.; Sun, X.; Peng, Y.; Wang, Y.; Xu, D.; Chen, W.; Wang, W.; Yan, X.; Ma, X. Intrinsic Properties Enabled Metal Organic Framework Micromotors for Highly Efficient Self-Propulsion and Enhanced Antibacterial Therapy. *ACS Nano* **2022**.

(31) Villa, K.; Novotný, F.; Zelenka, J.; Browne, M. P.; Ruml, T.; Pumera, M. Visible-Light-Driven Single-Component $BiVO_4$ Micromotors with the Autonomous Ability for Capturing Microorganisms. *ACS Nano* **2019**, 13 (7), 8135–8145.

(32) Pacheco, M.; Jurado-Sánchez, B.; Escarpa, A. Visible-Light-Driven Janus Microvehicles in Biological Media. *Angew. Chem. Int. Ed*. **2019**, 58 (50), 18017–18024.

(33) Rojas, D.; Kuthanova, M.; Dolezelikova, K.; Pumera, M. Facet Nanoarchitectonics of Visible-Light Driven Ag_3PO_4 Photocatalytic Micromotors: Tuning Motion for Biofilm Eradication. *NPG Asia Mater*. **2022**, 14 (1), 1–9

(34) Xu, L.; Gong, D.; Celi, N.; Xu, J.; Zhang, D.; Cai, J. Biohybrid Magnetic Microrobots for Enhanced Photocatalytic RhB Degradation and E.Coli Inactivation under Visible Light Irradiation. *Appl. Surf. Sci*. **2022**, 579, 152165.

(35) Ma, E.; Wang, K.; Hu, Z.; Wang, H. Dual-Stimuli-Responsive CuS-Based Micromotors for Efficient Photo-Fenton Degradation of Antibiotics. *J. Colloid Interface Sci*. **2021**, 603, 685–694.

(36) Ma, L.; Sun, T.; Cai, H.; Zhou, Z.-Q.; Sun, J.; Lu, M. Enhancing Photocatalysis in $SrTiO_3$ by Using Ag Nanoparticles: A Two-Step Excitation Model for Surface Plasmon-Enhanced Photocatalysis. *J. Chem. Phys*. **2015**, 143 (8), 084706.

(37) Xiao, Z.; Chen, J.; Duan, S.; Lv, X.; Wang, J.; Ma, X.; Tang, J.; Wang, W. Bimetallic Coatings Synergistically Enhance the Speeds of Photocatalytic TiO_2 Micromotors. *Chem. Commun*. **2020**, 56 (34), 4728–4731.

(38) Abd Elkodous, M.; Aatiqah, A.; Kawamura, G.; Tan, W. K.; Matsuda, A. Metallic Nanoparticles Loaded Al-$SrTiO_3$ Supported with $RhCr_2O_3$ and CoOOH Cocatalysts for Overall Water Splitting. *Int. J. Hydrogen Energy* **2022**.

(39) Linic, S.; Christopher, P.; Ingram, D. B. Plasmonic-Metal Nanostructures for Efficient Conversion of Solar to Chemical Energy. *Nat. Mater*. **2011**, 10 (12), 911–921.

(40) Lu, Z.; Rong, K.; Li, J.; Yang, H.; Chen, R. Size-Dependent Antibacterial Activities of Silver Nanoparticles against Oral Anaerobic Pathogenic Bacteria. *J. Mater. Sci. Mater. Med*. **2013**, 24 (6), 1465–1471.

(41) Liu, Y.; Xu, X.; Lv, S.; Li, H.; Si, Z.; Wu, X.; Ran, R.; Weng, D. Nitrogen Doped Graphene Quantum Dots as a Cocatalyst of $SrTiO_3$(Al)/CoOx for Photocatalytic Overall Water Splitting. *Catal. Sci. Technol*. **2021**, 11 (9), 3039-3046.

(42) Wang, X.; Sridhar, V.; Guo, S.; Talebi, N.; Miguel-López, A.; Hahn, K.; van Aken, P. A.; Sánchez, S. Fuel-Free Nanocap-like Motors Actuated under Visible Light. *Adv. Funct. Mater*. **2018**, 28 (25), 1705862.

(43) Liu, D.; Xue, C. Plasmonic Coupling Architectures for Enhanced Photocatalysis. *Adv. Mater*. **2021**,

33 (46), e2005738.

(44) Zeng, B.; Wang, S.; Feng, Z.; Xiao, Y.; Li, M.; Hong, F.; Zhao, Y.; Feng, Z.; Li, R.; Li, C. Atomically Unraveling the Dependence of Surface Microstructure on Plasmon-Induced Hydrogen Evolution on Au/$SrTiO_3$. *Nano Energy* **2022**, 91, 106638.

(45) Chen, Z.; Yin, H.; Wang, R.; Peng, Y.; You, C.; Li, J. Efficient Electron Transfer by Plasmonic Silver in $SrTiO_3$ for Low-Concentration Photocatalytic NO Oxidation. *Environ. Sci. Technol*. **2022**, 56 (6), 3604–3612.

(46) Zhang, Q.; Huang, Y.; Xu, L.; Cao, J.-J.; Ho, W.; Lee, S. C. Visible-Light-Active Plasmonic Ag-$SrTiO_3$ Nanocomposites for the Degradation of NO in Air with High Selectivity. *ACS Appl. Mater. Interfaces* **2016**, 8 (6), 4165–4174.

(47) Sridhar, V.; Podjaski, F.; Alapan, Y.; Kröger, J.; Grunenberg, L.; Kishore, V.; Lotsch, B. V.; Sitti, M. Light-Driven Carbon Nitride Microswimmers with Propulsion in Biological and Ionic Media and Responsive on-Demand Drug Delivery. *Sci. Robot*. **2022**, 7 (62), eabm1421.

Chapter 4

Conclusions

Compared with traditional nanoparticles, the controllable operation of nanomotors makes them have obvious advantages in dealing with practical problems in the fields of environmental governance and biomedicine. The use of photocatalytic materials and photoresponsive materials with excellent performance to fabricate light-driven nanomotors is the most important strategy to overcome defects and improve performance. In this dissertation, we introduce the application of light-driven nanomotors based on pure water splitting photocatalysts and photothermal materials with excellent performance in environmental governance and biomedicine. The use of single-atom catalysts or modified doped cocatalysts can greatly enhance the motion performance and application potential of photocatalytic nanomotors. In addition, photothermal nanomotors driven by near-infrared light also reflect their great advantages in biological applications. In the future, it is still the core task of the development of this field to continue to improve motor materials, improve the motor performance, and overcome its application defects.